Title: Unexpected growth of a classic yeast auxotroph

Authors: S. Branden Van Oss[1,2,7], Saurin Bipin Parikh[1,2,7], Nelson Castilho Coelho[1,2,7], Aaron Wacholder[1,2], Ivan Belashov[3], Manuel Michaca[1,2], Jiazhen Xu[1], Yun Pyo Kang [4,5], Katherine M. McCourt[1,2], Jake McKee[1], Trey Ideker[6], Andrew P. VanDemark[3], Gina M. DeNicola[4], Anne-Ruxandra Carvunis[1,2,*]

[1]Department of Computational and System Biology, University of Pittsburgh School of Medicine, Pittsburgh, Pennsylvania, 15213

[2]Pittsburgh Center for Evolutionary Biology and Medicine, University of Pittsburgh School of Medicine, Pittsburgh, Pennsylvania, 15213

[3]Department of Biological Sciences, University of Pittsburgh, Dietrich School of Arts & Sciences, Pittsburgh, Pennsylvania, 15213

[4]Department of Cancer Physiology, H. Lee Moffitt Cancer Center, Tampa, Florida, 33612

[5]College of Pharmacy and Research Institute of Pharmaceutical Sciences, Seoul National University, Seoul, Republic of Korea (current address)

[6]Departments of Medicine, Bioengineering, Computer Science and Engineering, Institute for Genomic Medicine, University of California San Diego, La Jolla, California, 92093

[7]Co-first author: These authors contributed equally

*Correspondence: anc201@pitt.edu

Keywords: microbiology, genetics, auxotrophy, methionine, hydrogen sulfide, sulfur, metabolism, conditional essentiality, *MET17*, homocysteine, microbial physiology

Corresponding Author:

Dr. Anne-Ruxandra Carvunis

Department of Computational and Systems Biology

Pittsburgh Center for Evolutionary Biology and Medicine

University of Pittsburgh School of Medicine

3501 Fifth Avenue

Pittsburgh, PA 15260, U.S.A.

Phone: +1 (412) 648-3335

Email: anc201@pitt.edu

ABSTRACT

In budding yeast, the Met15 enzyme has long been assumed to be the sole homocysteine synthase facilitating *de novo* synthesis of sulfur-containing organic compounds (organosulfurs) from inorganic precursors. Here we show that an alternative homocysteine synthase encoded by the previously uncharacterized gene YLL058W supports growth of mutants lacking *MET15* in the absence of exogenous organosulfurs. This growth is observed specifically when cells are deposited in an automated fashion to seed colonies, but not with traditional cell propagation techniques such as thick patches of cells or liquid cultures. We show that the lack of growth in these contexts, which has historically justified the status of *MET15* as a classic auxotrophic marker, is largely due to toxic levels of hydrogen sulfide accumulation rather than an inability to perform *de novo* homocysteine biosynthesis. These data suggest that cell fate decisions in yeast are influenced by hydrogen sulfide levels in the microenvironment. Our results have broad implications for investigations of sulfur metabolism, including studies of methionine restriction and aging.

17 The metabolism of organic sulfur-containing compounds ("organosulfurs") is critical for
18 all domains of life. There exists substantial diversity among the components of the
19 cellular networks that govern this metabolism. This is particularly true of plants and
20 microbes which, unlike animals, can synthesize organosulfurs from inorganic sulfates
21 via the sulfate assimilation pathway (SAP) (Thomas and Surdin-Kerjan, 1997). Enzymes
22 in the SAP reduce inorganic sulfates into sulfides and, in the terminal step, generate
23 homocysteine from O-acetyl-L-homoserine (OAH) and hydrogen sulfide (H_2S). In
24 *Saccharomyces cerevisiae*, Met15 (also referred to as Met17 and Met25) catalyzes this
25 reaction both *in vivo* (Masselot and De Robichon-Szulmajster, 1975) and *in vitro* (Chen
26 et al., 2018; Yamagata, 1971). Homocysteine can then be converted either directly to
27 methionine or indirectly to cysteine. These amino acids may be incorporated into
28 nascent polypeptides; alternatively, they may be modified to produce other essential
29 organosulfurs, including the "universal methyl donor" S-adenosylmethionine (SAM) and
30 glutathione, an important buffer against oxidative stress. Reactions downstream of
31 homocysteine biosynthesis are reversible; thus all of these organosulfurs may be
32 recycled back to homocysteine (Thomas and Surdin-Kerjan, 1997).
33
34 The first precise and complete deletion of *MET15* (*met15Δ0*) in *S. cerevisiae* was made
35 in 1998, in the S288C strain background, as part of a collection of "designer deletion"
36 strains containing one or more deletions of common auxotrophic markers (Brachmann
37 et al., 1998). Many commonly used laboratory strains contain this deletion, including
38 BY4741, which serves as the genetic background of the haploid *MAT***a** version of the
39 yeast deletion collection that has been extensively utilized for functional genomics and

40 other purposes (Douglas et al., 2012; Giaever and Nislow, 2014). The use of this
41 deletion as an auxotrophic marker, and the corresponding assumption that *MET15* is
42 required for growth in organosulfur-free media, has been applied to the interpretation of
43 a wide range of studies (Johnson and Johnson, 2014; Plummer and Johnson, 2019;
44 Zou et al., 2017).
45
46 Some data, however, suggest that *MET15* may not be strictly required for growth in the
47 absence of exogenous organosulfurs. *MET15* was first identified in a screen for
48 methylmercury resistance (Singh and Sherman, 1974). In this study, *met15* mutants
49 were shown to be auxotrophic for methionine and resistant to methylmercury, but, at a
50 critical concentration of methylmercury, the methionine requirement appeared to be
51 alleviated. There are also reports of papillae seen when replica plating thick patches of
52 *met15Δ0* cells to medium lacking organosulfurs (Boeke Lab, 2003).
53
54 Here, we demonstrate the existence of an alternative pathway for homocysteine
55 production in *S. cerevisiae*. We show that *met15Δ* cells grow robustly on media lacking
56 organosulfurs when propagated by automated colony transfer. This growth requires
57 exogenous inorganic sulfates and an intact SAP, as well as the uncharacterized gene
58 YLL058W. We demonstrate that Yll058w catalyzes homocysteine biosynthesis directly
59 from OAH and H_2S in a purified *in vitro* system. Hence, *met15Δ* cells can synthetize
60 organosulfurs from inorganic sulfates despite a long-held assumption to the contrary.
61 The ability of *met15Δ* cells to grow in the absence of exogenous organosulfurs is
62 context-dependent and highly sensitive to the way the cells are propagated. Specifically,

63 stable growth is observed with automated colony transfer, but very low or no growth is
64 observed when using conventional techniques such as thick patches or liquid cultures.
65 We show that this appearance of auxotrophy is at least partially explained by toxic
66 levels of accumulated H_2S. Our results have implications for a broad range of studies
67 that presume organosulfur auxotrophy in *met15Δ* cells, as well as for our understanding
68 of sulfur metabolism more generally.

RESULTS

met15Δ cells show unexpected growth in the absence of exogenous organosulfurs

We serendipitously observed robust growth of BY4741 when cells were automatedly transferred in a 384-colony array (**Figure 1A, Table S1**) from a rich medium (YPDA) to a "synthetic defined" (SD) medium lacking methionine (Met) and cysteine (Cys) and containing glucose as the carbon source (hereafter referred to as SD-Met+Glu). We first observed this using a BY4741 control strain from the haploid deletion collection, which has a *KanMX* cassette that confers resistance to the antibiotic Geneticin (G418). To confirm that this surprising finding was not unique to our stock of this strain or related to the presence of the *KanMX* cassette, we purchased BY4741 (lacking the cassette) and BY4742 (a *MET15*$^{+}$ control) from a commercial vendor (Dharmacon). These BY4741 cells again showed unexpected growth on SD-Met+Glu (**Figure 1B**). Both BY4741 and BY4742 harbor complete deletions of *URA3* and *LEU2* (Brachmann *et al.*, 1998), rendering them auxotrophic for uracil (Ura) and leucine (Leu). There was a large, statistically significant difference in relative colony size between BY4741 colonies that grew on SD-Met+Glu and the very small colonies detectable on SD-Ura+Glu or SD-Leu+Glu (**Figure 1C**; effect size = 0.627, p-value = 0.021 [Kruskal-Wallis test] and effect size = 0.757, p-value = 0.007 [Kruskal-Wallis test], respectively). These experiments reveal that, in this automated colony transfer procedure, BY4741 does not behave as an organosulfur auxotroph despite lacking *MET15*.

92 To confirm this unanticipated observation, we first ensured that our media were devoid
93 of organosulfur contamination. We analyzed both SD-Met and SD+Met media by mass
94 spectrometry, specifically looking for methionine, cysteine, homocysteine and SAM. No
95 contaminants were detected (**Table S2**). We next performed a cross between BY4741
96 and BY4742 and dissected eight four-spore tetrads. Monogenic phenotypes are
97 expected to exhibit 2:2 segregation in tetrads. When patched to SD-Met+Glu, we
98 observed such segregation in all eight tetrads, with two patches growing normally and
99 two patches displaying extremely weak growth, indicating that our observations were
100 not likely the result of an unknown secondary mutation (**Figure S1**). The extremely
101 weak growth of thick patches of cells lacking *MET15* was consistent with auxotrophy, in
102 contrast to the robust growth observed with the automated colony transfer. Thus, the
103 growth of cells lacking *MET15* on organosulfur-free media is dependent on how cells
104 are propagated.
105
106 To further investigate the impact of cell propagation technique on growth, we grew
107 BY4741 and BY4742 in liquid SD-Met+Glu medium (**Figure 1D**). In this context, very
108 little growth was seen in BY4741 cultures (**Figure 1E**). Drops taken from these cultures
109 were used to make spots and patches on SD-Met+Glu solid medium (**Figure 1D**). Here
110 again BY4741 cells displayed an auxotrophic-like phenotype, while BY4742 cells grew
111 normally (**Figure 1F**). Hence, BY4741 displays auxotroph-like growth when propagated
112 using traditional techniques.
113

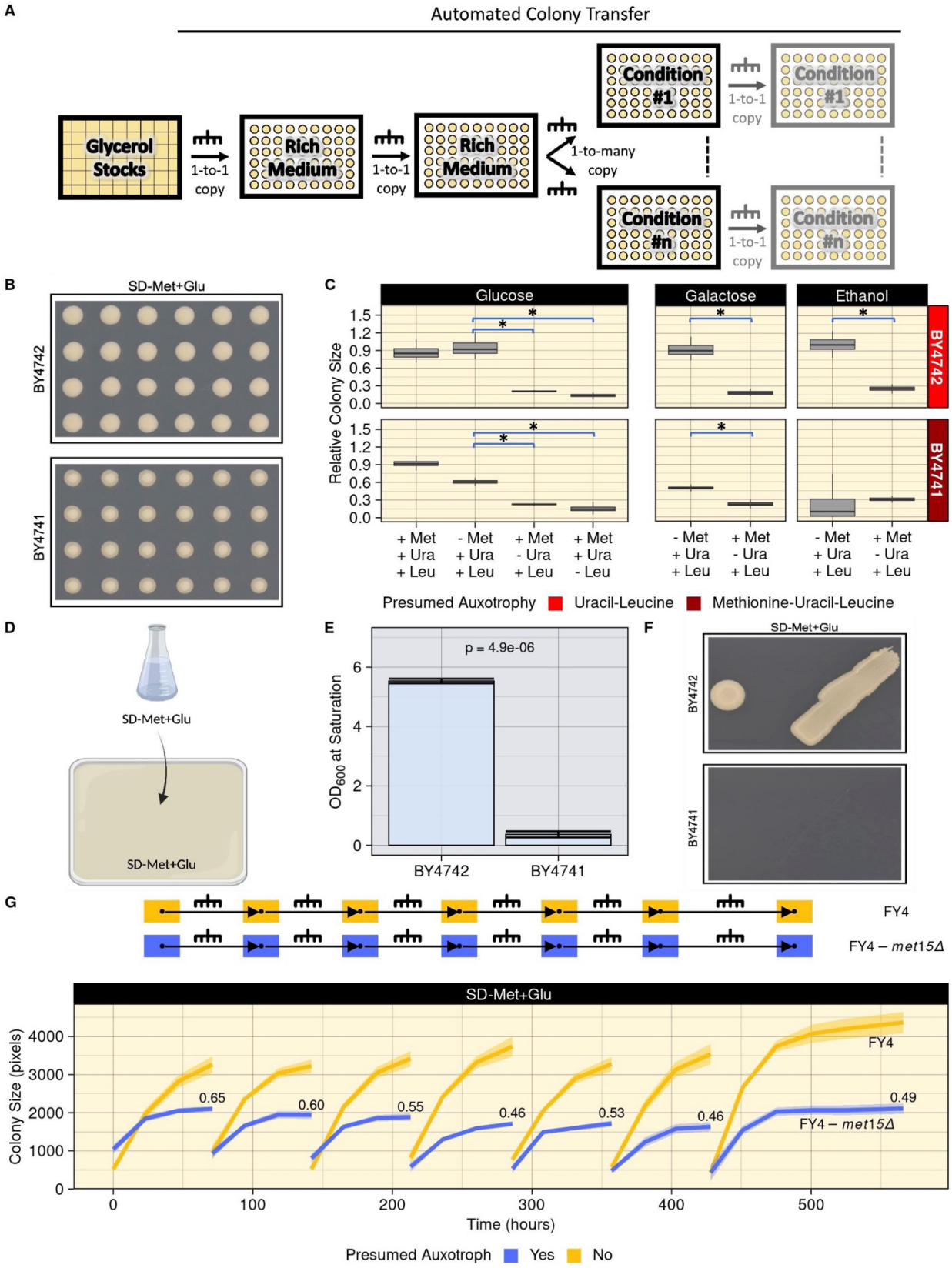
A
Automated Colony Transfer
Glycerol Stocks
1-to-1 copy
Rich Medium
1-to-1 copy
Rich Medium
1-to-many copy
Condition #1
1-to-1 copy
Condition #1
Condition #n
1-to-1 copy
Condition #n
B
SD-Met+Glu
BY4742
BY4741
C
Glucose
Galactose
Ethanol
Relative Colony Size
BY4742
BY4741
+ Met + Ura + Leu
- Met + Ura + Leu
+ Met - Ura + Leu
+ Met + Ura - Leu
- Met + Ura + Leu
+ Met - Ura + Leu
- Met + Ura + Leu
+ Met - Ura + Leu
Presumed Auxotrophy
Uracil-Leucine
Methionine-Uracil-Leucine
D
SD-Met+Glu
SD-Met+Glu
E
p = 4.9e-06
OD600 at Saturation
BY4742
BY4741
F
SD-Met+Glu
BY4742
BY4741
G
FY4
FY4 – met15Δ
SD-Met+Glu
Colony Size (pixels)
Time (hours)
0.65
0.60
0.55
0.46
0.53
0.46
0.49
FY4
FY4 – met15Δ
Presumed Auxotroph
Yes
No

Figure 1. The unexpected growth of *met15Δ* cells on organosulfur-free media is both stable and context-dependent. A) Automated colony transfer technique used in this study. See **Materials and Methods** and **Table S1**. For some experiments, cells were transferred to the condition plate once; for others, cells were transferred to the condition media multiple times (light gray plates). **B)** Unexpected growth of a strain harboring the *met15Δ0* deletion (BY4741) on a medium lacking organosulfurs (SD-Met+Glu). Cropped images of representative 384-density plates after 366 hours of growth are shown. See also **Figure S3A**. **C)** Robust growth of *met15Δ0* cells on SD-Met+Glu and SD-Met+Gal, but not on SD-Met+EtOH. Relative colony size distribution (y-axis) at saturation (~358 to 366 hours) of BY4742 and BY4741 grown on SD media with glucose, galactose or ethanol, and containing or lacking the indicated nutrients (x-axis). Relative colony size is normalized to the prototrophic FY4 grown in the same conditions (**Figure S3B; Materials and Methods**). *: significant Kruskal-Wallis test (p-value < 0.05) comparing the median relative colony sizes of biological replicates between two strains. **D)** Experimental setup for traditional cell propagation techniques used in this study (see **Materials and Methods**). **E)** BY4741 cells fail to grow in liquid SD-Met+Glu medium. Mean OD_{600} after ~51 hours in SD-Met+Glu liquid cultures (y-axis) over three biological replicates for each strain (x-axis). Error bars: standard error. p: two-tailed Student's T-test. **F)** BY4741 cells fail to grow on solid SD-Met+Glu medium in large spots or patches. Cropped representative images of cells grown for 192 hours are shown. **G)** Growth of FY4-*met15Δ* on an organosulfur-free medium is stable over six consecutive automated colony transfers. Top: experimental design for comparing the growth of FY4-*met15Δ* (blue) and FY4 (yellow) over consecutive transfers on SD-Met+Glu. Bottom: colony size (y-axis) over time (x-axis). Lines represent the mean colony size at each time point. Shaded area: one standard deviation. Numbers next to the blue curves indicate the fitness of FY4-*met15Δ* relative to FY4 as determined by dividing median colony sizes at the final time point of each curve.

We next interrogated the extent to which the unexpected growth of BY4741 colonies depends on the specific composition of the growth medium. We repeated the automated colony transfer procedure using SD-Met and SD-Ura media with either galactose (SD-Met+Gal and SD-Ura+Gal) or ethanol (SD-Met+EtOH and SD-Ura+EtOH) as the carbon source (**Figure 1C**). Similar to our observations in SD-Met+Glu, when galactose was used as a carbon source, BY4741 colonies grew to much larger sizes on SD-Met+Gal than on SD-Ura+Gal (effect size = 0.561, p-value =0.021 [Kruskal-Wallis test]). In contrast, the miniscule growth of BY4741 on SD-Met+EtOH was consistent with auxotrophy. We also repeated the procedure using "synthetic complete" (SC) medium containing all amino acids except Met and Cys (SC-Met-Cys). We observed robust growth of BY4741 cells similar to that seen on SD-Met, whether glucose or galactose was used as a carbon source (**Figure S2**). As was the case with SD media, the growth

152 of BY4741 colonies on SC-Leu+Glu was substantially weaker than was growth on SC-
153 Met-Cys+Glu (**Figure S2;** effect size = 0.914, p-value = 0.007 [Kruskal-Wallis test]).
154
155 To study the specific consequences of *MET15* loss independent of the other
156 auxotrophies present in BY4741, we used CRISPR to make a scarless deletion of
157 *MET15* in the prototrophic FY4 background (FY4-*met15Δ*) (see **Materials and**
158 **Methods**) and used this strain for all subsequent experiments. Similarly to BY4741,
159 FY4-*met15Δ* cells grew robustly when automatically transferred on SD-Met with glucose
160 or galactose, but not ethanol, used as carbon sources (**Figure S3B**). FY4-*met15Δ* also
161 grew similar to BY4741 on SC-Met-Cys medium whether glucose or galactose was
162 used (**Figure S2**). Thus, the unexpected growth of cells lacking *MET15* is not
163 dependent on the genetic background particular to BY4741.
164
165 To determine whether the robust growth of *met15Δ* colonies may be explained by
166 *met15Δ* recycling and/or scavenging of preexisting organosulfurs, we transferred FY4-
167 *met15Δ* from and to SD-Met+Glu six consecutive times. FY4-*met15Δ* cells displayed
168 robust growth on SD-Met+Glu over repeated transfers (**Figure 1G**). Relative to FY4, the
169 fitness of these colonies was 0.65 on the initial SD-Met+Glu plates and stabilized at
170 ~0.50. The amount of new biomass generated throughout this experiment demonstrates
171 that the growth of FY4-*met15Δ* cells cannot be explained by recycling or scavenging.
172 Despite a longstanding assumption of auxotrophy, *met15Δ* strains can in fact grow
173 stably in media lacking organosulfurs. This growth is context-dependent, manifesting
174 when cells are grown by automated colony transfer, but not in thick patches or liquid

175 cultures, and when cells utilize glucose or galactose, but not ethanol, as a carbon
176 source.
177
178 **Stable growth of *met15Δ* cells on organosulfur-free media requires inorganic**
179 **sulfates and is not seen in other presumed auxotrophs**
180 To investigate whether the growth of *met15Δ* colonies that we observed in our
181 automated colony transfer assay was specific to *met15Δ* mutants, we again used
182 CRISPR to make complete deletions in the FY4 background of nine additional genes
183 encoding enzymes involved in organosulfur biosynthesis (**Figure 2A)**. These mutants,
184 along with FY4 and the FY4-*met15Δ* strain, were transferred as described above
185 (**Figure 1A**) to either YPDA or SD-Met+Glu plates.
186
187 All mutant strains displayed growth (or lack thereof) on SD-Met+Glu that was consistent
188 with current knowledge of organosulfur biosynthesis (**Figure 2B**), with the exception of
189 FY4-*met3Δ.* In agreement with previous studies (Masselot and De Robichon-
190 Szulmajster, 1975; Ono et al., 1988), the FY4-*met5Δ,* FY4-*met10Δ,* FY4-*met2Δ*, FY4-
191 *met6Δ*, FY4-*met13Δ*, and FY4-*cys4Δ* strains all displayed negligible or no growth on
192 SD-Met+Glu (effect sizes = 0.887, 0.869, 0.930, 0.904, 0.903, and 0.981, respectively;
193 p-value < 0.05 [Kruskal-Wallis test] for all comparisons) (**Figure 2B**). The extent to
194 which *str3Δ* mutants can utilize sulfates has not, to our knowledge, been directly
195 examined, and loss of *MET12* has not been associated with any *in vivo* phenotypes
196 (Raymond et al., 1999). The FY4-*str3Δ* strain had a moderate growth defect in SD-

197 Met+Glu that was also observed in YPDA, while the FY4-*met12Δ* strain grew normally
198 (**Figure 2B**). Only the FY4-*met3Δ* mutant displayed an unexpected growth phenotype.
199
200 Met3 catalyzes the first step in the reduction of intracellular sulfate and is thought to be
201 essential for growth when unreduced sulfates are the sole sulfur source (Masselot and
202 De Robichon-Szulmajster, 1975); however, the FY4-*met3Δ* mutant displayed growth on
203 SD-Met+Glu that was roughly equivalent to that seen with the FY4-*met15Δ* strain
204 (relative to FY4, effect size = 0.651, p-value < 0.001 [Kruskal-Wallis test] and effect size
205 = 0.618, p-value < 0.001 [Kruskal-Wallis test], respectively; **Figure 2B**). The growth of
206 FY4-*met3Δ* was largely unaffected by carbon source, with only a slightly greater growth
207 defect in SD-Met+Gal and SD-Met+EtOH than in SD-Met+Glu (effect size = 0.289, p-
208 value = 0.021 [Kruskal-Wallis test] and effect size = 0.298, p-value = 0.021 [Kruskal-
209 Wallis test] respectively, **Figure S4**).

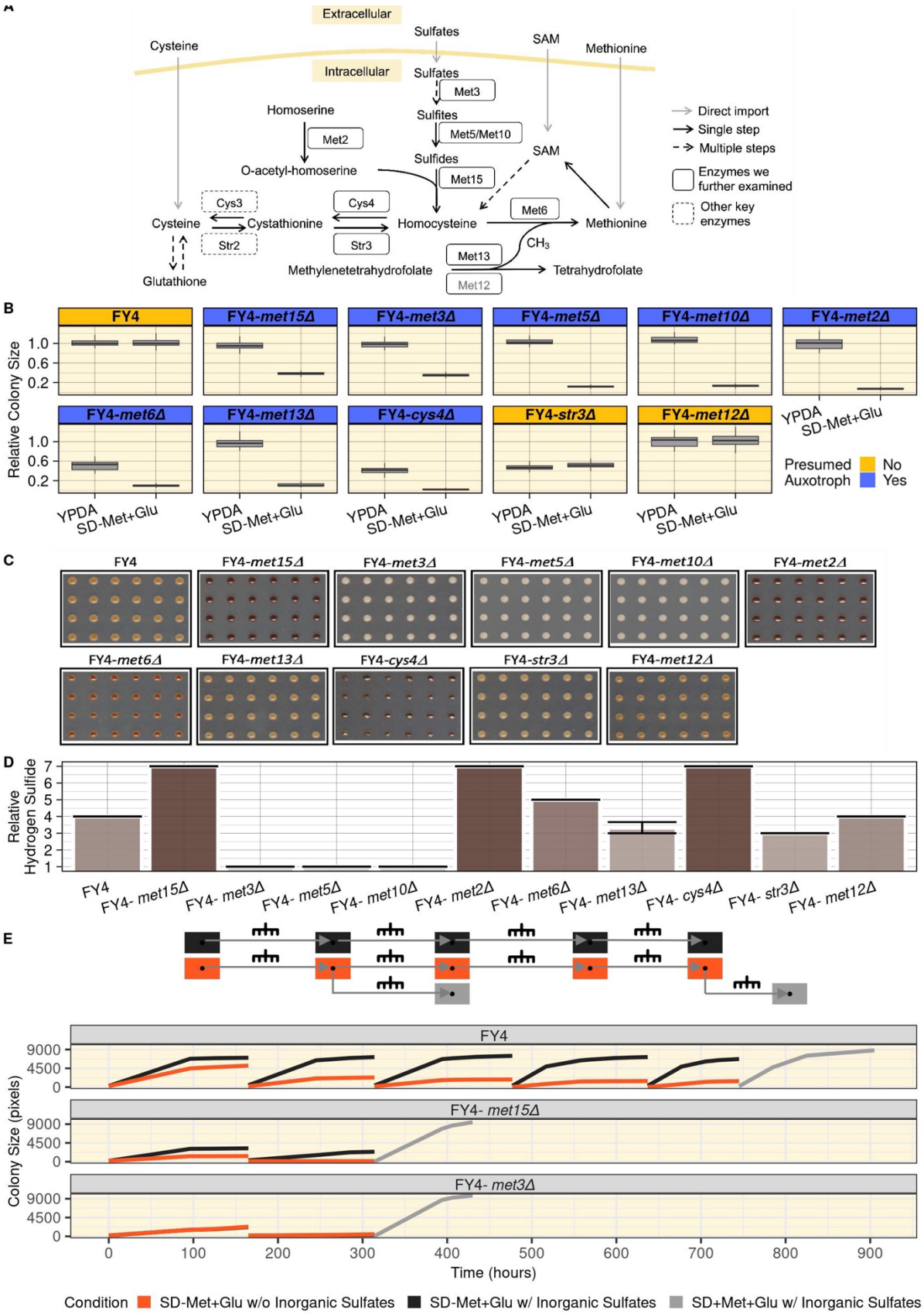
A
Extracellular
Intracellular
Cysteine
Sulfates
SAM
Methionine
Sulfates
Met3
Homoserine
Sulfites
Met5/Met10
Met2
SAM
O-acetyl-homoserine
Sulfides
Met15
Cys3
Cys4
Met6
Cysteine
Cystathionine
Homocysteine
Methionine
Str2
Str3
CH3
Met13
Glutathione
Methylenetetrahydrofolate
Tetrahydrofolate
Met12
Direct import
Single step
Multiple steps
Enzymes we further examined
Other key enzymes
B
FY4
FY4-met15Δ
FY4-met3Δ
FY4-met5Δ
FY4-met10Δ
FY4-met2Δ
FY4-met6Δ
FY4-met13Δ
FY4-cys4Δ
FY4-str3Δ
FY4-met12Δ
Relative Colony Size
1.0
0.6
0.2
YPDA
SD-Met+Glu
Presumed Auxotroph
No
Yes
C
FY4
FY4-met15Δ
FY4-met3Δ
FY4-met5Δ
FY4-met10Δ
FY4-met2Δ
FY4-met6Δ
FY4-met13Δ
FY4-cys4Δ
FY4-str3Δ
FY4-met12Δ
D
Relative Hydrogen Sulfide
7
6
5
4
3
2
1
FY4
FY4- met15Δ
FY4- met3Δ
FY4- met5Δ
FY4- met10Δ
FY4- met2Δ
FY4- met6Δ
FY4- met13Δ
FY4- cys4Δ
FY4- str3Δ
FY4- met12Δ
E
FY4
FY4- met15Δ
FY4- met3Δ
Colony Size (pixels)
9000
4500
0
0
100
200
300
400
500
600
700
800
900
Time (hours)
Condition
SD-Met+Glu w/o Inorganic Sulfates
SD-Met+Glu w/ Inorganic Sulfates
SD+Met+Glu w/ Inorganic Sulfates

210

211 **Figure 2. Growth of *met15Δ* colonies in organosulfur-free media is specific and dependent on the**
212 **utilization of inorganic sulfates. A)** The *S. cerevisiae* organosulfur biosynthesis pathway. Exogenous
213 organosulfurs such as methionine, cysteine, and SAM can be directly imported (gray arrows); inorganic
214 sulfates can also be imported and reduced to sulfides via the SAP. Sulfides are converted into
215 organosulfurs by Met15, which catalyzes *de novo* homocysteine biosynthesis. Homocysteine is then
216 converted to numerous critical downstream organosulfurs, a selection of which are indicated. The *in vivo*
217 biosynthesis of methionine requires both the methionine synthase Met6 and the
218 methylenetetrahydrofolate reductase Met13. The Met13 isozyme, Met12 is shown in gray. Enzymes are
219 indicated within boxes, next to the reactions they catalyze, which are illustrated with arrows that indicate
220 reaction directionality. Drawing inspired by (Walvekar and Laxman, 2019). **B)** *met3Δ* cells also show
221 unexpected growth. Cells grown in each condition as described in **Figure 1A** and **Materials and**
222 **Methods**. Box plots show the growth of FY4 and its derivative mutant deletion strains, on rich medium
223 (YPDA, left) and on medium lacking organosulfurs (SD-Met+Glu, right). The box plots show relative
224 colony size data (y-axis; see **Materials and Methods**) per strain (subpanels) at saturation (~83.5-89.0
225 hours in YPDA; 160.0-173.5 hours in SD-Met+Glu). **C-D)** Disruptions of the organosulfur biosynthesis
226 pathway result in a range of H_2S accumulation in cells. Representative crops of 384-density plate images
227 (Panel C) and qualitative assessment, by eye, of relative H_2S (Panel D) in the strains transferred to rich
228 medium containing bismuth for ~160-173.5 hours (BiGGY; see **Table S9**). Error bars: standard error. **E)**
229 Growth of FY4-*met15Δ* colonies requires inorganic sulfates. This experimental procedure is indicated in
230 the schema at the top of the panel. The initial transfer steps were as described in **Figure 1A** The
231 indicated strains were then grown either on SD-Met+Glu medium containing inorganic sulfates (black) or
232 on an analogous medium completely devoid of inorganic sulfates (orange) (see **Materials and Methods**
233 and **Supplementary Material**). After reaching saturation, all strains were transferred to the same
234 condition. Beneath the schema are growth curves (colony size, y-axis) of the indicated strains
235 (subpanels) through the entire experimental procedure (time, x-axis) with the mean colony size depicted.
236 The orange (SD-Met+Glu) and black curves (SD-Met+Glu) in the lower subpanel (FY4-*met3Δ*) overlap.
237

238 This surprising growth of *met3Δ* cells led us to examine the level of free sulfides present
239 in our mutant strains. To do so we utilized a colony color assay using bismuth. Bismuth
240 reacts with free sulfides to form a dark precipitate on the surface of cells. (Nickerson,
241 1953). The darkness of the colonies is therefore a proxy readout for *de novo*
242 homocysteine biosynthesis through the canonical pathway, with strains deficient in this
243 activity expected to accumulate sulfides, as well as for the activity of the SAP, where a
244 broken or inefficient pathway would be expected to result in little to no sulfide
245 accumulation. The strains fell loosely into three groups. The FY4-*met15Δ* and FY4-
246 *met2Δ* mutants both formed very dark colonies when grown on complete media
247 containing bismuth (BiGGY), confirming that they are deficient in homocysteine
248 biosynthesis. The FY4-*cys4Δ* mutant also formed very dark colonies, consistent with the
249 upregulation of the SAP that occurs when cells cannot make cysteine (Hansen and

250 Johannesen, 2000). The FY4-*met6Δ,* FY4-*met13Δ*, and FY4-*str3Δ* mutants formed an
251 intermediate amount of precipitate, as did the FY4 control and the FY4-*met12Δ* mutant.
252 Finally, the FY4-*met3Δ*, FY4-*met5Δ*, and FY4-*met10Δ* mutants had no discernable
253 precipitate (**Figures 2C-D**), confirming that the SAP is indeed disrupted in these strains
254 as expected. We saw consistent results in a bismuth-containing medium lacking
255 organosulfurs (SD-Met+Glu+Bi; **Figure S5**). Altogether, these observations are
256 consistent with the known roles of the deleted genes in organosulfur biosynthesis
257 (**Figure 2A**). Therefore, the unexpected growth of FY4-*met15Δ* and FY4-*met3Δ* cells is
258 not explained by previous mischaracterizations of the positions of the Met15 and Met3
259 enzymes in the organosulfur biosynthesis pathway.
260
261 To determine whether the surprising growth of FY4-*met15Δ* and FY4-*met3Δ* cells in
262 media lacking organosulfurs depends on the utilization of inorganic sulfates, we
263 examined how these mutants grown when automatically transferred onto plates entirely
264 devoid of both organosulfurs and inorganic sulfates. We observed reduced, but not
265 abolished, growth in SD-Met+Glu without inorganic sulfates for FY4-*met15Δ* and FY4
266 control colonies. In contrast, the growth of FY4-*met3Δ* colonies was unaffected by the
267 presence or absence of inorganic sulfates (**Figure 2E**). We then transferred cells from
268 SD-Met+Glu with or without inorganic sulfates to the same medium a second time.
269 Upon so doing, the growth of the FY4-*met15Δ* strain on the no sulfate medium was
270 essentially abolished, indicating that said growth depends on the utilization of inorganic
271 sulfates. The FY4-*met3Δ* strain failed to show any substantial growth upon a second
272 transfer, irrespective of the presence or absence of inorganic sulfates. Therefore, unlike

273 the stable growth seen in FY4-*met15Δ* colonies, the growth of FY4-*met3Δ* colonies
274 observed after a single transfer to organosulfur-free media is not stable (**Figure 2E**).
275 Altogether, these results demonstrate that the unexpected stable growth of *met15Δ*
276 cells is not observed when other key enzymes in the pathway are missing, and requires
277 inorganic sulfates.
278
279 To determine whether the cells that stopped growing when deprived of inorganic
280 sulfates had arrested or died, we asked whether we could restore growth by transferring
281 them to SD medium containing both methionine and sulfates. Growth was restored for
282 both the FY4-*met15Δ* and FY4-*met3Δ* strains that had previously stopped growing
283 (**Figure 2E**). An increase in colony size was also observed for FY4, which had
284 surprisingly continued to grow on media lacking both organosulfurs and inorganic
285 sulfates even after five successive transfers albeit to a significantly reduced colony size
286 (**Figure 2E**). These data are consistent with studies showing that cells starved for
287 inorganic sulfates and other natural nutrients tend to arrest rather than die (Boer et al.,
288 2008).
289
290 **YLL058W is critical for the growth of organosulfur-starved *met15Δ* cells**
291 Our findings led us to hypothesize that the *S. cerevisiae* genome encoded at least one
292 enzyme other than Met15 capable of catalyzing *de novo* homocysteine biosynthesis.
293 We therefore examined the targets of the sole known transcriptional activator of the
294 sulfur metabolic network, Met4. Of the 45 genes that compose the Met4 “core regulon”
295 (Lee et al., 2010), six constituted possible candidates: three that are classified by the

296 Saccharomyces Genome Database (SGD) as “uncharacterized,” and three that are
297 classified as verified genes but have functions described as “unknown” or “putative”
298 (Stanford University, 2020). Sequence analyses placed two of these candidates –
299 YHR112C and YLL058W - as a part of the PLP-dependent transferase superfamily,
300 together with *MET15* and nine other genes primarily involved in sulfur metabolism
301 (Wilson et al., 2009). Of these two genes, YLL058W was the more compelling candidate
302 due to the additional fact that its encoded protein is predicted to have the ability to
303 catalyze homocysteine biosynthesis by a yeast genome-scale metabolic model (Wang
304 et al., 2021).
305
306 YLL058W is located near the telomere of chromosome 12 within a cluster of genes that
307 are transcriptionally regulated by Met4, several of which have a direct role in sulfur
308 metabolism (**Figure 3A)** (Lee *et al.*, 2010). There has been speculation that it may have
309 arisen as a result of horizontal transfer (Lee *et al.*, 2010) - a relatively rare occurrence in
310 yeast. We thus pursued further investigation of the YLL058W ORF, beginning with its
311 evolutionary origins. YLL058W has two close paralogs in the *S. cerevisiae* genome:
312 *STR2*, which encodes an enzyme that converts cysteine into cystathionine (**Figure 2A**),
313 and the uncharacterized YML082W, which is a copy of *STR2* generated during the
314 whole-genome duplication event (Byrne and Wolfe, 2005). We identified bacterial or
315 fungal homologs of YLL058W, *STR2,* and YML082W using BLASTP and HMMER
316 (Eddy, 2011) and performed K-means clustering on these sequences. If YLL058W were
317 derived from a recent horizontal transfer event, we would expect it to be more similar to
318 some of its homologs outside *Ascomycota* than to its *Ascomycota* homologs. Instead,

319 all homologs outside *Ascomycota* grouped together along with all budding yeast
320 homologs more distantly related to *S. cerevisiae* than the *Hanseniaspora* genus. The
321 homologs found in all descendants of the common ancestor of *Saccharomyces* and
322 *Hanseniaspora* comprised two additional groups, one containing YLL058W and the
323 other containing both *STR2* and YML082W (**Figure S6**). The genes belonging to the
324 YLL058W class and the *STR2*/YML082W class appear at approximately the same point
325 in the phylogenetic tree (**Figure 3B**), prior to whole-genome duplication. Therefore, the
326 most plausible evolutionary scenario is duplication of an ancestral gene into YLL058W
327 and the *STR2/*YML082W ancestor, followed by substantial divergence of both copies
328 from the ancestral state, and later by duplication of the *STR2/*YML082W ancestor.
329 Interestingly, in all species that contain genes of the YLL058W class, the YLL058W
330 homolog is located near the telomeres among a collection of other sulfur metabolism
331 related genes (**Figure 3A and Table S3**). The preservation of this pattern in the
332 genomically-unstable near-telomere region is consistent with a strong selective
333 constraint keeping YLL058W in proximity to other genes involved in sulfur metabolism.

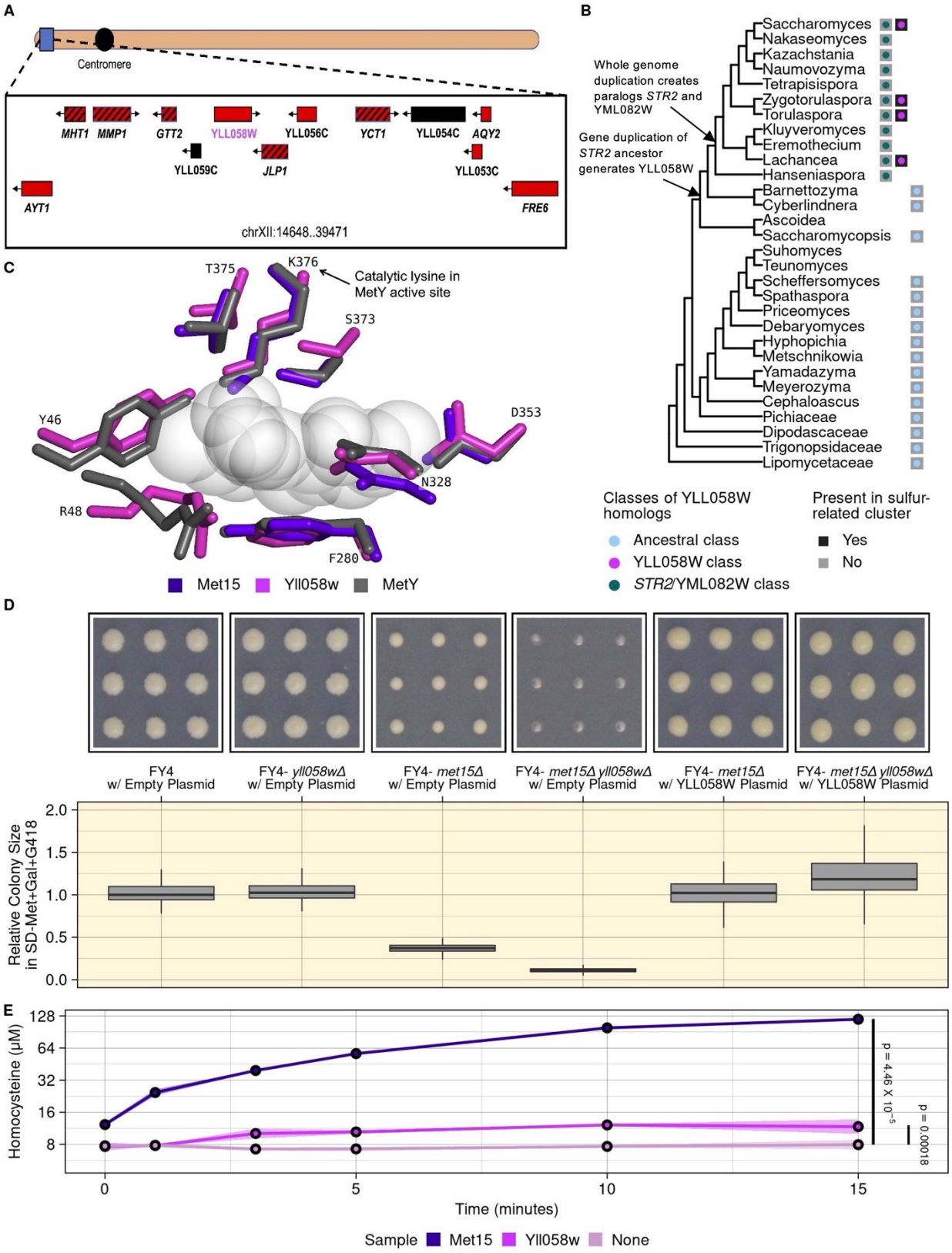
A
Centromere
MHT1
MMP1
GTT2
YLL058W
YLL056C
YCT1
YLL054C
AQY2
YLL059C
JLP1
YLL053C
AYT1
FRE6
chrXII:14648..39471
B
Whole genome duplication creates paralogs STR2 and YML082W
Gene duplication of STR2 ancestor generates YLL058W
Saccharomyces
Nakaseomyces
Kazachstania
Naumovozyma
Tetrapisispora
Zygotorulaspora
Torulaspora
Kluyveromyces
Eremothecium
Lachancea
Hanseniaspora
Barnettozyma
Cyberlindnera
Ascoidea
Saccharomycopsis
Suhomyces
Teunomyces
Scheffersomyces
Spathaspora
Priceomyces
Debaryomyces
Hyphopichia
Metschnikowia
Yamadazyma
Meyerozyma
Cephaloascus
Pichiaceae
Dipodascaceae
Trigonopsidaceae
Lipomycetaceae
Classes of YLL058W homologs
Ancestral class
YLL058W class
STR2/YML082W class
Present in sulfur-related cluster
Yes
No
C
T375
K376
Catalytic lysine in MetY active site
S373
Y46
D353
N328
R48
F280
Met15
Yll058w
MetY
D
FY4 w/ Empty Plasmid
FY4- yll058wΔ w/ Empty Plasmid
FY4- met15Δ w/ Empty Plasmid
FY4- met15Δ yll058wΔ w/ Empty Plasmid
FY4- met15Δ w/ YLL058W Plasmid
FY4- met15Δ yll058wΔ w/ YLL058W Plasmid
Relative Colony Size in SD-Met+Gal+G418
2.0
1.5
1.0
0.5
0.0
E
Homocysteine (μM)
128
64
32
16
8
p = 4.46 X 10−5
p = 0.00018
0
5
10
15
Time (minutes)
Sample
Met15
Yll058w
None

334
335

Figure 3. Yll058w functions as an inefficient homocysteine synthase. A) Genomic context of YLL058W (Stanford University, 2020). In *S. cerevisiae*, YLL058W (magenta) is located near a cluster of genes that are transcriptionally activated by Met4 ((Lee *et al.*, 2010); red boxes), several of which have a direct role in sulfur metabolism (red boxes with black stripes). Black boxes indicate ORFs that fall into neither category. **B)** Distribution of YLL058W homolog clusters across the budding yeast phylogenetic tree. The tree topology follows (Shen et al., 2018). Circles adjacent to each taxon indicate whether YLL058W homologs belonging to each of the three classes identified by K-means clustering in the MDS plot (**Figure S6**; see **Materials and Methods**) are found in the genome of that taxa, while black boxes indicate the presence of a cluster of sulfur-related genes, such as is depicted in Panel A for *S. cerevisiae*. **C)** Yll058w has structural similarity to a homocysteine synthase. Structural overlap of MetY from *Thermatoga maritima* (PDB ID: 7KB1) (gray) with the predicted structure of Yll058w (magenta) and Met15 (violet) calculated using AlphaFold. For clarity, only the active site residues are shown. An O-acetyl-homoserine derivative reaction intermediate captured within the MetY structure (Brewster et al., 2021) is shown in semi-transparent spheres. Residue labeling corresponds to the Yll058w sequence. See also **Figure S7**. **D)** Yll058w is critical for growth in the absence of *MET15*. The indicated strains (x-axis) bearing high-copy (2μ ORI) plasmids conferring resistance to G418, and, where indicated, overexpressing YLL058W, were grown on SD-Met+Gal+G418 medium. The box plots show relative colony size (y-axis) data at saturation (336 hours). Cropped, representative images of the plates corresponding to the strains tested are shown on top. See also **Figure S8**. **E)** Yll058w catalyzes homocysteine biosynthesis. An *in vitro* homocysteine biosynthesis assay was carried out using recombinantly expressed, purified *S. cerevisiae* Met15 (violet) or Yll058w (magenta), or a no-enzyme control (pink), as the catalyst (see **Materials and Methods**). Homocysteine levels (y-axis) were measured at various time points (x-axis). Solid lines: mean. Shaded area: one standard deviation. p: two-tailed, paired Student's T-test paired combining all replicates and time points. Homocysteine levels were significantly higher than the negative control for both Met15 ($p=4.46 \times 10^{-5}$) and Yll058w ($p=0.00018$). The y-axis is shown on a log2 scale.

The sequence similarity and evolutionary relationship of Yll058w to enzymes involved in sulfur metabolism led us to examine its predicted structure. To do so, we utilized the crystal structure of MetY (**Figure S7A**), a bacterial *O*-acetylhomoserine aminocarboxypropyltransferase that catalyzes the homocysteine biosynthesis from *O*-acetylhomoserine and bisulfide (Brewster *et al.*, 2021), as well as the predicted structures of Met15 and Yll058w generated by AlphaFold2 (Jumper et al., 2021). The MetY crystal structure captured a reaction intermediate, allowing for a precise determination of active site residues. The predicted structures of both Met15 and Yll058w are highly similar to the experimentally determined structure of MetY within the active site, including the catalytic lysine (**Figures 3C and S7B**). One difference is position 280 in the Yll058w sequence, which is a phenylalanine in Yll058w but a tyrosine in both Met15 and MetY. Another difference in the overall fold is that MetY and

374 Met15 function as homotetramers (Brewster *et al.*, 2021; Yamagata, 1976), with
375 multimerization domains allowing the distinct monomers to come together to complete
376 the active site (**Figure S7C**). In contrast, Yll058w lacks a multimerization domain and is
377 predicted to be monomeric. However, it contains an approximately 180 amino acid
378 region before the catalytic domain that has no homology to MetY or Met15. This region
379 folds back onto the core of the protein, supplying the missing amino acids to the active
380 site (**Figure S7D**). Altogether, these comparative structural analyses suggest that a
381 Yll058w monomer may be capable of carrying out catalysis similar to that of the MetY
382 and Met15 tetramers.
383
384 We thus sought to determine whether the putative Yll058w enzyme is necessary and
385 sufficient to support the growth of *met15Δ* cells in the absence of exogenous
386 organosulfurs using genetic approaches. We used CRISPR to delete YLL058W in the
387 FY4 background, and made a *met15Δ yll058wΔ* double mutant in the same
388 background. We also constructed high copy-number plasmids overexpressing
389 YLL058W. The FY4-*yll058wΔ* single mutant resulted in only a very modest growth
390 defect on SD-Met+Glu (effect size = 0.054, p-value > 0.05 [Kruskal-Wallis test]) (**Figure**
391 **S8A**), and when grown on bismuth-containing medium displayed an intermediate level
392 of precipitate (**Figure S8B-C**); its relatively normal growth and intermediate H_2S
393 accumulation was comparable to FY4 and FY4-*met12Δ* (**Figures 2B-D and S5A-B**).
394 Strikingly however, the FY4-*met15Δ yll058wΔ* double mutant showed little to no growth
395 in the absence of exogenous organosulfurs (**Figure 3D**), indicating a synthetic lethal
396 interaction between *MET15* and YLL058W. To verify that this effect was due to the loss

397 of the YLL058W gene product, we compared the growth of FY4-*met15Δ* and FY4-
398 *met15Δyll058wΔ* strains carrying an empty vector plasmid to the same strains carrying
399 a plasmid overexpressing YLL058W. Overexpression of YLL058W in the FY4-
400 *met15Δyll058wΔ* background resulted in a large, statistically significant increase in
401 growth (**Figure 3D**; effect size= 9.478, p-value < 0.001 [Kruskal-Wallis test]).
402 Overexpression of YLL058W also significantly enhanced the growth of the FY4-*met15Δ*
403 single mutant (effect size= 1.703, p-value < 0.001 [Kruskal-Wallis test]) (**Figure 3D**).
404 This strongly suggests that the growth of *met15Δ* cells in the absence of exogenous
405 organosulfurs is mediated by the putative enzyme encoded by YLL058W.
406
407 To directly examine the ability of Yll058w to catalyze homocysteine biosynthesis, we
408 purified recombinant protein from *E. coli*, along with Met15 as a positive control, and
409 carried out *in vitro* reactions (see **Materials and Methods**). This assay uses the
410 canonical O-acetyl-homoserine and H_2S substrates and includes in the reaction mixture
411 pyridoxal 5'-phosphate (PLP), a cofactor critical for Met15 activity. Yll058w was able to
412 catalyze homocysteine production significantly above background, albeit much less
413 efficiently than Met15, with the Met15 reactions yielding ~9.9 times as much
414 homocysteine at the 15-minute time point (**Figure 3E**). Thus, YLL058W does encode an
415 alternative homocysteine synthase capable of catalyzing the same reaction as Met15.
416
417 We sought to investigate whether such inefficient *de novo* homocysteine biosynthesis
418 would be sufficient to support growth in the absence of Met15 using metabolic
419 modeling. To do so, we adapted an enzyme-constrained version of Yeast8, the current

420 consensus genome-scale metabolic model in *S. cerevisiae* (Lu et al., 2019) (see
421 **Materials and Methods**). We first removed all of the hypothetical Yll058w-"consuming"
422 reactions and replaced them with our observed *in vitro* reaction. This had little effect on
423 the flux of the biomass equation, a proxy for growth in this *in silico* system. We next
424 removed *MET15* from the model and evaluated the flux through the biomass equation at
425 a range of arbitrarily assigned catalytic efficiencies (Kcat) for Yll058w. We found that an
426 appreciable reduction in biomass occurred only when Yll058w was assigned a catalytic
427 efficiency ~100x lesser than that assigned to Met15 in the model (**Figure S9**). These
428 simulations, together with our structural, *in vivo*, and biochemical findings, demonstrate
429 that it is plausible that Yll058w activity enables cells to grow in the absence of *MET15*.
430

431 **Removal of H_2S enhances the growth of *met15Δ* cells in organosulfur-free media**

432 Our observations (**Figure 1C-F**) show that *met15Δ* cells do indeed display auxotrophic-
433 like phenotypes when propagated using the type of conventional methods that were
434 almost exclusively in use at the time of the gene's initial characterization, such as liquid
435 cultures in flasks or thick patches on Petri dishes, and that these same cells also fail to
436 grow when ethanol is used as a carbon source. It may be that *met15Δ* cells fail to grow
437 in these contexts not due to organosulfur starvation *per se*, but to some downstream
438 cause brought about by the loss of Met15 activity. One such cause may be the large
439 excess of H_2S present in *met15Δ* cells (**Figures 2C-D and S5A-B**). This accumulation
440 of H_2S is expected in *met15Δ* cells since the reaction catalyzed by Met15 is one of the
441 major sulfide-consuming reactions in the cell (Linderholm et al., 2008). Although some

442 amount of H_2S is required for cell growth, at high levels it is toxic (Blackstone et al.,
443 2005).
444
445 To investigate whether the auxotroph-like behavior of *met15Δ* cells propagated in liquid
446 cultures or thick patches might be partly due to toxic levels of H_2S, we examined the
447 growth of FY4 and FY4-*met15Δ* cells in liquid SD-Met+Glu cultures with or without the
448 H_2S chelator ferric (Fe)-EDTA, which bonds free sulfides that exit the cell by diffusion
449 (Gaensly et al., 2014; Philip and Brooks, 1974) (**Figure 4A**). In the presence of Fe-
450 EDTA, we observed a striking increase in the growth of FY4-*met15Δ* cultures (p-value =
451 0.01 [Student's t-test]; **Figure 4B**, top right panel). To rule out spontaneous mutations
452 as the reason for this growth increase, we repassaged the cultures in SD-Met+Glu
453 medium lacking chelator (**Figure 4A**). The repassaged FY4-*met15Δ* cultures showed
454 little to no growth (**Figure 4B**, bottom right panel). Interestingly, FY4 cultures that had
455 previously been propagated in the presence of chelator saturated at a higher OD_{600} than
456 those that had not (p-value = 0.0012 [Student's t-test]; **Figure 4B**, bottom left panel).
457 We then placed cells from both the original and the repassaged cultures on solid media
458 plates in large drops and patches (**Figures 4A and 4C**). The FY4-*met15Δ* cells failed to
459 grow on SD-Met+Glu and SC-Met-Cys+Glu in drops or patches, irrespective of their
460 previous exposure to the chelator (**Figure 4C**). These results demonstrate that the
461 growth of FY4-*met15Δ* cultures in the presence of chelator is not facilitated by heritable
462 mutations.
463

464 Drops and patches of FY4-*met15Δ* cells on BiGGY plates retained the expected dark
465 brown color (**Figure 4C**). This indicates that the cells are still producing an excess of
466 H_2S in the absence of the chelator, suggesting that the chelator also failed to induce
467 epigenetic or other heritable changes affecting H_2S levels. However, upon adding Fe-
468 EDTA to the solid medium, the lack of growth of drops and patches of FY4-*met15Δ* cells
469 in organosulfur-free media was partially rescued (**Figure 4C**). Thus, the growth defect
470 (in some settings) and auxotrophic-like behavior (in other settings) of *met15Δ* cells
471 grown without organosulfurs is at least partially attributable to H_2S toxicity.

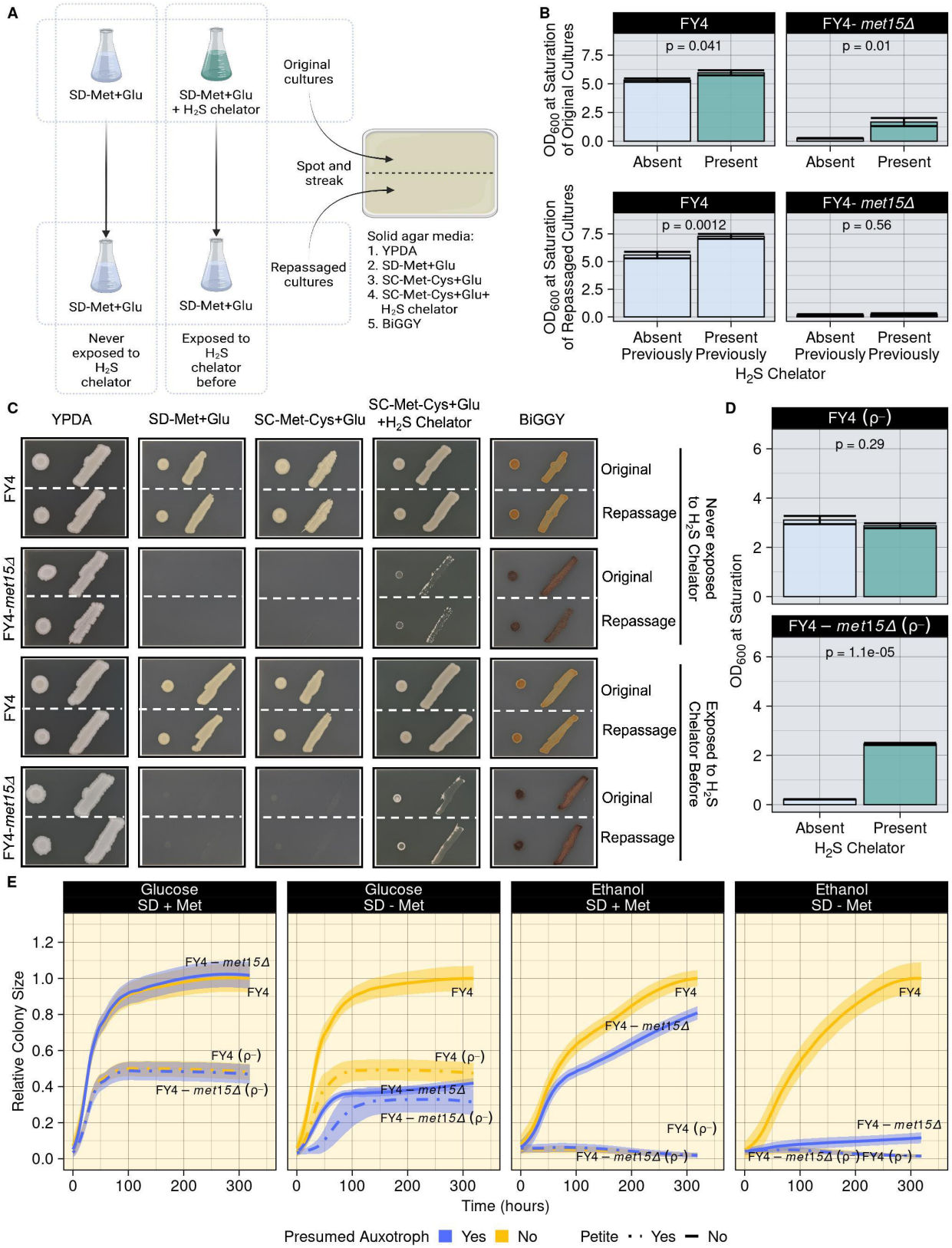
A
SD-Met+Glu
SD-Met+Glu + H2S chelator
Original cultures
Spot and streak
Repassaged cultures
SD-Met+Glu
SD-Met+Glu
Solid agar media:
1. YPDA
2. SD-Met+Glu
3. SC-Met-Cys+Glu
4. SC-Met-Cys+Glu+ H2S chelator
5. BiGGY
Never exposed to H2S chelator
Exposed to H2S chelator before
B
FY4
FY4- met15Δ
p = 0.041
p = 0.01
p = 0.0012
p = 0.56
OD600 at Saturation of Original Cultures
OD600 at Saturation of Repassaged Cultures
Absent
Present
Absent Previously
Present Previously
H2S Chelator
C
YPDA
SD-Met+Glu
SC-Met-Cys+Glu
SC-Met-Cys+Glu +H2S Chelator
BiGGY
FY4
FY4-met15Δ
Original
Repassage
Never exposed to H2S Chelator
Exposed to H2S Chelator Before
D
FY4 (ρ⁻)
FY4 – met15Δ (ρ⁻)
p = 0.29
p = 1.1e-05
OD600 at Saturation
Absent
Present
H2S Chelator
E
Glucose SD + Met
Glucose SD - Met
Ethanol SD + Met
Ethanol SD - Met
Relative Colony Size
FY4 – met15Δ
FY4
FY4 (ρ⁻)
FY4 – met15Δ (ρ⁻)
Time (hours)
Presumed Auxotroph Yes No
Petite Yes No

Figure 4. Chelation of H_2S facilitates the growth of *met15Δ* cells in the absence of exogenous organosulfurs. A) Experimental setup. Strains were grown in Erlenmeyer flasks in either SD-Met+Glu or SD-Met+Glu+Fe-EDTA liquid media (top two flasks, original cultures). Once saturation was reached for all cultures, those cultures were then repassaged in SD-Met+Glu media (bottom two flasks, repassaged cultures) and again grown to saturation (Panel B). Ten μl from each culture were then spotted and struck to the indicated solid media (Panel C). See also **Figure S11**. **B)** The H_2S chelator Fe-EDTA partially rescues the growth of *met15Δ* cells grown in liquid media. Mean OD_{600} values of the cultures after ~51 hours of growth with or without chelator (top), and ~51 hours after repassage (bottom). Error bars: standard error; p: two-tailed, unpaired Student's t-test. Individual values for each replicate, from both independent experiments, are shown in **Table S4**; outlier FY4-*met15Δ* cultures that showed unexpected growth in SD-Met+Glu were excluded from the data presented here and indicated in green text in the table. **C)** Chelation of H_2S partially rescues the growth of FY4-*met15Δ* cells grown in spots or streaks. Cropped, representative images of cells grown for 192 hours are shown (see **Panel A** and **Materials and Methods**). **D**) Growth defect on media lacking organosulfurs of *met15Δ* petite (ρ^-) derivatives is rescued in presence of H_2S chelator. FY4 and the FY4-*met15Δ* petite (ρ^-) derivatives were grown in similar fashion as the original cultures from Panel A. Data is represented as in Panel B. **E)** A growth defect of *met15Δ* cells grown with ethanol is seen in the presence and absence of organosulfurs in the media. Growth curves of FY4 and the FY4-*met15Δ* mutant (solid line), along with their respective petite (ρ^-) derivatives (dashed line), grown on SD media containing or lacking methionine and utilizing either glucose or ethanol as the sole carbon source are shown. For each condition (subpanel) the cells were grown as described in **Figure 1A and Materials and Methods**. All colony sizes were normalized to the median colony size of FY4 at the final time point in the same condition. Line: mean relative colony size. Shaded regions: one standard deviation. **Table S5** contains the Kruskal-Wallis Test results comparing the growth of a particular strain as estimated by area under the curve in the presence or absence of methionine in media containing either glucose or ethanol as the carbon source.

Excess H_2S is often associated with mitochondrial dysfunction (Paul et al., 2021). Yeast strains with damaged or absent mitochondrial genomes display what is known as the petite phenotype (Ferguson and von Borstel, 1992). To determine whether the partial rescue of *met15Δ* cells by an H_2S chelator is dependent on the mitochondrial genome, we constructed petite (ρ-) derivatives of FY4 and FY4-*met15Δ* (see **Materials and Methods**) and grew them in SD-Met+Glu cultures with or without Fe-EDTA. We observed a strong rescue of FY4-*met15Δ* ρ- growth upon addition of the chelator (p-value = 1.1 $X10^{-5}$ [Student's t-test]; **Figure 4D**, bottom panel). We next transferred these strains and their respective non-petite parental strains to solid media containing or lacking methionine, and with either glucose or ethanol as the carbon source (**Figure 4E**). In SD medium containing methionine, non-petite FY4-*met15Δ* cells grew poorly relative to their *MET15*$^+$ counterparts when ethanol was used as the carbon source. Still,

512 FY4-*met15Δ* ρ- strains grew on SD-Met+Glu almost as well as their non-petite parental
513 strains. These results suggest that *met15Δ* cells experience some degree of
514 mitochondrial dysfunction that impairs their ability to metabolize ethanol, but that neither
515 their unexpected growth in automated colony transfer settings, nor the chelator-
516 mediated rescue of their lack of growth in traditional propagation techniques, require a
517 functional mitochondrial genome.

518 **DISCUSSION**

519

520 Here we show that, contrary to longstanding assumptions, the organosulfur auxotrophy-
521 like phenotype in a *met15Δ* background is context-dependent. Our analyses
522 demonstrate that the *S. cerevisiae* genome, and possibly those of several closely
523 related fungal species, encode another enzyme, the previously uncharacterized
524 Yll058w, that can catalyze the same reaction as Met15, albeit less efficiently. This
525 activity compensates for the loss of *MET15* and enables the growth of *met15Δ* cells in
526 the absence of exogenous organosulfurs when cells are propagated using automated
527 colony transfer or grown in the presence of an H_2S chelator. Altogether, our
528 observations support a model according to which *met15Δ* cells can synthesize enough
529 homocysteine to support growth through the activity of Yll058w, but experience chronic
530 H_2S toxicity that prevents growth in certain contexts (**Figure 5**). Given its evolutionary
531 conservation, Yll058w may well have other biological activities that are not investigated
532 here.

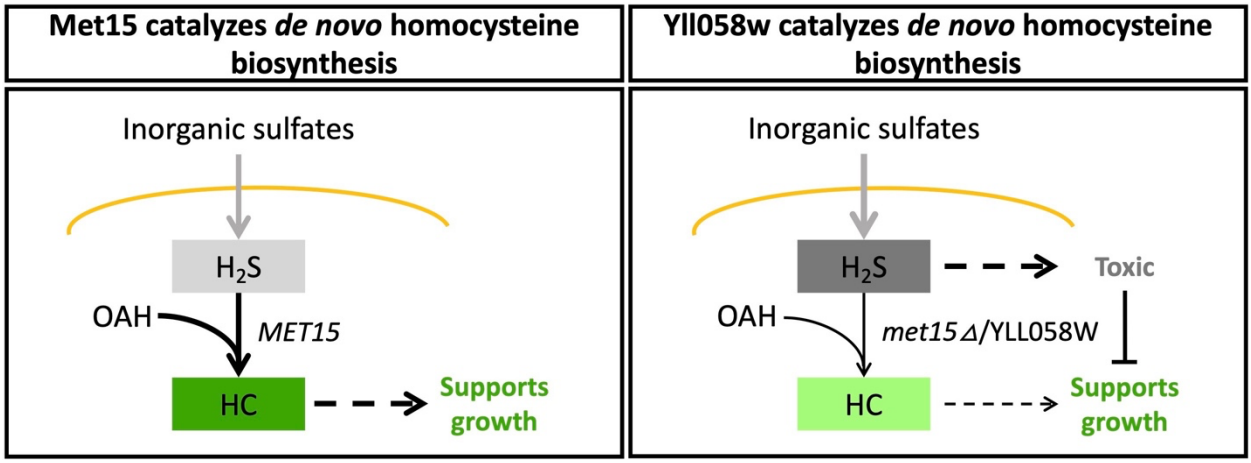

Figure 5. H_2S toxicity inhibits growth when Yll058w catalyzes *de novo* homocysteine biosynthesis. Model representing the hypothesized response to organosulfur starvation in cells containing or lacking *MET15*. Extracellular inorganic sulfates are imported through the cell membrane (yellow line) and reduced to H_2S. When Met15 is present (left), cells efficiently convert H_2S and O-acetylhomoserine (OAH) into homocysteine, leading to a moderate amount of H_2S (light gray) and an adequate amount of homocysteine (HC; dark green) to support normal growth. When Met15 is absent, homocysteine biosynthesis is catalyzed by the comparatively inefficient Yll058w enzyme (right). The resulting lower amount of homocysteine (light green) is sufficient to support growth in some contexts, but the high amount of H_2S that accumulates (dark gray), exacerbated by an upregulated intake of sulfates, can become toxic and lead to cell death or arrest in other contexts.

H_2S-mediated context-dependence of a classic auxotrophy

H_2S levels are extremely high when *met15Δ* cells are growing without exogenous organosulfurs (**Figure S5**), and our results indicate that H_2S toxicity is at least partially responsible for the arrest and/or death that occurs in *met15Δ* cells grown using conventional techniques (**Figure 5**). A primary mechanism for the toxic effects of elevated H_2S, seen in many organisms, involves mitochondrial disfunction (Paul *et al.*, 2021). The failure of *met15Δ* cells to utilize ethanol (**Figures 1C, 4E, and S3B**) is consistent with mitochondrial dysfunction. However, the ability of the H_2S chelator Fe-EDTA to restore the growth of petite FY4-*met15Δ* cells grown in liquid cultures (**Figure 4D**), as well as the ability of these cells to grow on solid SD-Met+Glu medium (**Figure 4E**), strongly suggests that H_2S is limiting the growth of *met15Δ* cells in part through a pathway that does not involve the mitochondrial genome. The precise molecular

558 mechanisms at play may be dissected in future genome-scale investigations of
559 suppressor and synthetic lethal mutations, similar to how a recent study dissected the
560 mechanisms underlying the growth defect associated with petites (Vowinckel et al.,
561 2021).
562
563 We show that *met15Δ* cells behave like organosulfur auxotrophs under conventional
564 growth techniques, but not when propagated by automated colony transfer. We
565 hypothesize that robust growth is possible in an automated colony transfer context
566 because excess sulfides can be eliminated through diffusion between the evenly
567 spaced small colonies whereas, in the context of thick patches of cells, excess sulfides
568 are secreted and affect neighboring cells, creating group-level toxicity and self-limiting
569 growth. Similarly, we hypothesize that H_2S toxicity is high in liquid cultures because the
570 semi-sealed environment limits gas exchange. While the conditional essentiality of
571 genes has been well studied in the context of differing genetic backgrounds or
572 environments (Hou et al., 2018; Zhang and Ren, 2015), to our knowledge, *MET15*
573 represents the first report of a case in which the essential nature of gene is dependent
574 on the way cells are propagated.
575
576 **An expanded yeast sulfur metabolic network**
577 Sulfur-containing amino acids act as cellular sensors for growth control (Laxman et al.,
578 2013; Sutter et al., 2013). There has therefore been renewed interest in sulfur
579 metabolism. In particular, methionine restriction is known to increase longevity in a
580 broad range of organisms (Green et al., 2021), and may serve as a therapeutic

581 treatment for certain cancers (Endicott et al., 2021). Mutants lacking *MET15* have been
582 widely used in the study of lifespan extension in yeast (Johnson and Johnson, 2014;
583 Plummer and Johnson, 2019; Ruckenstuhl et al., 2014; Zou *et al.*, 2017). Our data add
584 a potential layer of nuance to such studies and hint at the possibility of a role for H_2S in
585 lifespan extension. More generally, our discovery of the alternative homocysteine
586 synthase Yll058w may influence the interpretation of the plethora of published studies,
587 including genome-wide screens conducted in the BY4741 background, wherein the
588 results or methodologies assumed *met15Δ* cells to be auxotrophic for organosulfurs.
589 Our findings that *S. cerevisiae* can grow in the absence of exogenous organosulfurs
590 despite very low levels of *de novo* homocysteine biosynthesis, that the previously
591 observed auxotroph-like phenotypes are dependent on cell propagation techniques, and
592 that H_2S levels control group-level growth behaviors, may represent a novel avenue for
593 studying the interplay between sulfur metabolism and its many dependent phenotypes.
594
595 It is of note that even the prototrophic FY4 strain displayed enhanced growth in liquid
596 media when cells were previously exposed to an H_2S chelator (**Figure 4B**). This
597 suggests that 1) even wild-type cells suffer some degree of H_2S-induced stress when
598 grown in organosulfur-free media, and 2) removal of excess H_2S allows the cells to
599 adapt to this stress, likely at the level of gene expression or epigenetics. This may have
600 implications for anyone seeking to maximize cellular growth in media lacking, or
601 containing low amounts of, organosulfurs, whether in an industrial or a research setting.
602 Also surprising was the limited, but continued, growth of FY4 cells even after multiple
603 successive transfers to media lacking both organosulfurs and inorganic sulfates (**Figure**

604 **2E**). This continued growth was not anticipated given that to our knowledge the SAP
605 relies on inorganic sulfates (**Figure 2A**). Perhaps Met15, but not Yll058w, can
606 metabolize derivatives of other sulfur-containing compounds present in our growth
607 media (*e.g.* biotin). Altogether, our work suggests there may yet be more unknown
608 factors that contribute to the yeast sulfur metabolic network.

609 **MATERIALS AND METHODS**

610 **Yeast strains**

611 The well-characterized S288C-derived *Saccharomyces cerevisiae* strains FY4, BY4741
612 and BY4742 were used throughout this work (Brachmann *et al.*, 1998; Winston et al.,
613 1995).

614

615 **CRISPR/Cas9 deletion strains**

616 All other strains (**Table S6**) were derived by CRISPR/Cas9 based scarless whole-ORF
617 deletions of genes from the prototrophic strain, FY4. Co-transformations were made
618 with 5μg of repair fragment and 1μg of plasmid expressing cas9 (Addgene 60847,
619 **Table S7**) (Ryan et al., 2014) with the respective sgRNA (DiCarlo et al., 2013).
620 Identification of PAM sites and sgRNA selection were chosen using Benchling
621 (https://www.benchling.com/) and the sgRNA and repair fragment sequences are given
622 in **Table S8**. Transformed cells were plated on YPDA+G418 and colonies were PCR
623 genotyped to select those with the correct gene deletion. The positive clones were then
624 grown on YPDA to induce the loss of the cas9- and sgRNA-containing plasmids. Strains
625 carrying plasmids for overexpression experiments were made with the LiAc/PEG/ssDNA
626 protocol (Dunham, 2015) using 500ng of each plasmid and selected on YPDA+G418.

627

628 **Petite strains**

629 Petite derivatives of FY4 and FY4-*met15Δ* were made using a slightly modified version
630 of the standard LiAc/PEG/ssDNA yeast transformation protocol (Dunham, 2015), with

631 shorter incubation times and without a DNA template, followed by replica platting on
632 YPDA and YP-Glycerol plates to identify the petites.
633
634 **Strain stock plates**
635 Stock plates were constructed for each strain by selecting four independent colonies
636 from streakouts, which were used to inoculate liquid YPDA medium and grown
637 overnight at 30ºC. These cultures were considered biological replicates. The cultures
638 were then used to create 384-well glycerol stocks (glycerol 25% v/v) for each strain,
639 with each biological replicate occupying one-fourth of the plate, distributed uniformly.
640
641 **Plasmid construction**
642 The overexpression plasmids used in **Figure 3D** were made by replacing the Leu2 gene
643 by KanMx cassette into the destination plasmid pAG425GPD-ccdB (Alberti, 2007). This
644 plasmid was used as an empty vector plasmid (pARC0112, **Table S7**) while an LR
645 recombination (Gateway LR Clonase II Enzyme Mix, ThermoFisher) of this same
646 plasmid with an entry clone containing the ORF YLL058W was used to produce the
647 plasmid overexpressing YLL058W (pARC0172, **Table S7**).
648
649 Plasmids pARC0190 and pARC0191 (**Table S7**) were made by amplification of *MET15*
650 and YLL058W coding sequences, respectively, from FY4 genomic DNA, and cloned into
651 a pET28a-derived vector expressing an N-terminal, cleavable 10XHis-Ruby tag (Kredel
652 at.al., 2009).
653

654 **Growth Media**

655 The recipes for all the various growth media used in this study are given in **Table S9**.
656 When required, the analogous liquid medium was made with the same composition,
657 excluding the agar.

658

659 **Strain Crossing**

660 The cross depicted in **Figure S1** was carried out by standard techniques. Briefly, the
661 BY4741 and BY4742 deletion collection parent strains (**Table S6**) were mated on YPDA
662 solid medium and incubated at room temperature (RT) for ~6 hours, and then struck to
663 select for colonies formed from single diploids on solid SD+His+Leu+Ura medium
664 **(Table S9)**. After incubation at 30°C for ~2 days on the diploid selection medium,
665 colonies were patched to "GNA" plates (**Table S9**) and incubated at 30°C for ~2 days.
666 These plates were then replica plated to "sporulation (SPO)" medium (**Table S9)**
667 containing histidine, lysine, methionine, uracil, and leucine, and incubated at RT for ~11
668 days. Four-spore tetrads were selected and dissected using standard techniques and
669 initially grown on YPDA. Individual spores were then patched to petri dishes as shown
670 in **Figure S1**.

671

672 **Automated Colony Transfer**

673 Using the benchtop RoToR HDA robotic plate handler (Singer Instruments Co Ltd,
674 Roadwater, UK) strains were transferred from glycerol stocks to solid rich medium
675 plates (YPDA, **Table S9**) as described on **Figure 1A** and incubated at 30°C for 72
676 hours (see **Table S1** for a description of the settings used). Each of these plates were

677 copied to two YPDA plates, which represented the two technical replicates of plates per
678 strain, and again incubated at 30°C for 48 hours. This step reduces the variability in
679 colony size that is introduced when cells are transferred from glycerol stocks. Finally,
680 these plates were 'one-to-many' copied onto various solid 'condition' media plates (**see**
681 **Table S9)** depending on the experiment. The plates were incubated at 30°C and
682 periodically imaged until the colonies reached saturation. This experimental protocol,
683 depicted in **Figure 1A**, was carried out at least twice per experiment to control for batch
684 effect. **Figures 1C, 1G, 2B, 2E, 3D and 4E** (indicated with a dull yellow background) as
685 well as **Figures S2, S3B, S4 and S8A** were carried out in this manner.
686
687 **Colony size estimation**
688 Serial imaging of the plates was done either using spImager Automated Imaging
689 System (S & P Robotics Inc., Ontario, Canada) or manually using a custom-made
690 lightbox with an overhead camera mount using a commercially available SLR camera
691 (18Mpixel Rebel T6, Canon USA Inc., Melville, NY, USA). The plates were imaged at
692 regular intervals beginning right after transfer until the colonies reached saturation. The
693 images were analyzed in bulk using a custom script made using functions from the
694 MATLAB Colony Analyzer Toolkit (Bean et al., 2014) to provide colony size estimations
695 (https://github.com/sauriiiin/lid_personal/blob/master/justanalyze.m). The output files
696 containing colony size information along with the images is available at
697 https://bit.ly/3pOe6aT.
698
699

700 **Relative fitness measurement**

701 A spatially cognizant colony size database was built using the colony size estimates per
702 the LI Detector framework for high-throughput colony-based screening analysis (Parikh
703 et al., 2021). For all experiments, first, the outermost border colonies were removed
704 from the dataset because these usually tend to grow more due to excess access to
705 nutrients, leaving a maximum of 77 colony size observations per strain per time point
706 per plate per biological replicate. Outlier colony size values per experiment per technical
707 replicate per time point per plate per biological replicate were removed using two
708 median adjusted deviations as a cutoff. These raw colony size values are reported in
709 **Figures 1G** and **2E**.

710

711 For **Figures 1C**, **2B**, **3D, 4E, S2, S3B, S4,** and **S8A,** the median colony size per time
712 point of the prototrophic strain, FY4, was used to calculate relative colony size of every
713 colony per strain per time point. At saturation, the relative colony size distribution per
714 strain is determined by the median relative colony sizes per plate per biological
715 replicate. This relative colony size distribution is compared amongst strains using the
716 non-parametric Kruskal-Wallis Test to determine significant changes in fitness. Effect
717 size values are calculated as the difference in median colony sizes divided by the
718 median colony size of the strain being used as reference in the comparison.
719 Additionally for **Figure 4E and Table S5**, growth curve analysis was done with the
720 *growthcurver (Sprouffske and Wagner, 2016)* package in R (Team, 2021), using the
721 time series colony size data per colony per strain per technical replicate per biological
722 replicate. This time series data was first converted into an equally spaced time series

723 using a second degree locally weighed scatterplot smoothing (loess) function to
724 generate 100 equally spaced data points. This was then fed into the
725 '*SummarizeGrowthByPlate()*' function of the gro*wthcurver* package (Sprouffske and
726 Wagner, 2016) to make estimates of the area under the curve (AUC) per colony per
727 strain in the experiment. AUC summarizes a growth curve by integrating the
728 contributions of the initial population size, growth rate, and carrying capacity into a
729 single value, making it a more robust estimation of growth-curve-based 'fitness.'
730 Relative area under the curve, effect sizes and significant changes were estimated the
731 same way as the colony size data described above. The AUCs from the data in **Figure**
732 **4E** were used to calculate the statistics in **Table S5**.
733

734 **Relative H_2S measurement**

735 Bismuth containing plates (BiGGY and SD-Met+Glu+Bi; **Table S9**) were used to assess
736 the level of excess sulfides in various strains. Cells were transferred from YPDA plates
737 onto bismuth containing plates, as described on **Figure 1A**. The qualitative assessment
738 involved two replicates scored by eye in duplicate by independent observers on a scale
739 of 1-7, with the darkest strain(s) assigned a value of seven and the lightest strains
740 assigned a value of one.
741

742 **Mass spectrometry analysis of media by semi-targeted high-resolution LC-HRMS**

743 **<u>Sample preparation</u>**

744 Metabolic quenching and polar metabolite pool extraction was performed by adding
745 400µL ice cold methanol to 100µL of sample. Deuterated (D_3)-creatinine and (D_3)-

746 alanine, (D_4)-taurine and (D_3)-lactate (Sigma-Aldrich) was added to the sample lysates
747 as an internal standard for a final concentration of 10μM. Samples were vortexed, and
748 then homogenized using a 25°C water bath sonicator for 5 minutes. The supernatant
749 was then cleared of protein by centrifugation at 16,000xg. Two μL of cleared
750 supernatant was subjected to online LC-MS analysis.
751
752 **LC-HRMS Method**
753 Analyses were performed by untargeted LC-HRMS. Briefly, Samples were injected via a
754 Thermo Vanquish UHPLC and separated over a reversed phase Thermo HyperCarb
755 porous graphite column (2.1×100mm, 3μm particle size) maintained at 55°C. For the 20
756 minute LC gradient, the mobile phase consisted of the following: solvent A (water /
757 0.1% formic acid) and solvent B (ACN / 0.1% formic acid). The gradient was the
758 following: 0-1min 1% B, increase to 15%B over 5 minutes, continue increasing to 98%B
759 over 5 minutes, hold at 98%B for five minutes, reequillibrate at 1%B for five minutes.
760 The Thermo IDX tribrid mass spectrometer was operated in positive ion mode, scanning
761 in $ddMS^2$ mode (2 μscans) from 70 to 800 m/z at 120,000 resolution with an AGC target
762 of 2e5 for full scan, 2e4 for ms^2 scans using HCD fragmentation at stepped 15,35,50
763 collision energies. Source ionization setting was 3.0kV spray voltage for positive mode.
764 Source gas parameters were 35 sheath gas, 12 auxiliary gas at 320°C, and 8 sweep
765 gas. Calibration was performed prior to analysis using the Pierce™ FlexMix Ion
766 Calibration Solutions (Thermo Fisher Scientific). Integrated peak areas were then
767 extracted manually using Quan Browser (Thermo Fisher Xcalibur ver. 2.7)

768 (Metabolomics & Lipidomics Core, University of Pittsburgh Health Sciences Core
769 Research Facilities).
770
771 **Evolutionary origins of YLL058W**
772 Genome sequences of 332 budding yeasts were taken from a published dataset (Shen
773 *et al.*, 2018). Each genome was scanned for ORFs (consisting of the sequence between
774 an ATG start codon and a stop codon in the same frame) larger than 300 bp. We then
775 used BLASTP on the predicted protein products of these ORFs to identify the strongest
776 match among *S. cerevisiae* annotated genes. BLASTP was run with default settings and
777 a 10^{-4} e-value cutoff. All ORFs for which the best match (i.e., the lowest BLASTP e-
778 value) was either the *S. cerevisiae* YLL058W sequence or the sequence of one of its
779 two *S. cerevisiae* homologs (*STR2* and YML082W) were retained. For each ortholog
780 identified, we also noted the best *S. cerevisiae* matches for the 5 nearest ORFs in each
781 direction that had a match. To supplement this list with orthologs from more distant
782 species, we submitted the *S. cerevisiae* YLL058W sequence to the HMMER homology
783 search tool (Eddy, 2011). From these results, we selected the strongest matching
784 sequences (lowest e-values) from a variety of bacterial and fungal taxa outside of the
785 *Ascomycota* phylum (four bacterial and nine fungal outgroups). The full list of YLL058W
786 homologs and their sequences is given in **Supplementary File 1**.

787 We next constructed a multiple alignment of all homologs using the MUSCLE aligner
788 (Madeira et al., 2019). We used the R package bio2mds to perform K-means clustering
789 on the sequence alignment and to visualize the results using multidimensional scaling.
790 To investigate the phylogenetic distribution of each cluster within budding yeasts, we

791 used the phylogeny generated by the same study of budding yeasts that formed the
792 foundation of our sequence dataset (Shen *et al.*, 2018).
793

794 **Purification of recombinantly expressed proteins**

795 Both Met15 or Yll058w were expressed as fusion proteins with an N-terminal His_{10}-
796 mRuby2 tag which can be removed by cleavage with TEV protease. Fusion proteins
797 were expressed in the BL21 (DE3) RIPL CodonPlus *E. coli* strain (Stratagene). Cells
798 were grown at room temperature in 2L of standard LB media containing kanamycin and
799 chloramphenicol to an OD600 of ~0.6, induced with 0.5mM IPTG, and grown for eight
800 additional hours at room temperature post-induction. Purification of both proteins was
801 performed essentially as described previously (Van Oss et al., 2016). Briefly, both
802 proteins were purified by two rounds (pre- and post-cleavage with TEV protease) of
803 nickel affinity chromatography followed by ion exchange chromatography. Met15 was
804 further purified by size exclusion chromatography. The final purified fractions that were
805 used in the *in vitro* homocysteine assay are shown in **Figure S10**.
806

807 ***in vitro* homocysteine assay**

808 *in vitro* homocysteine biosynthesis was carried out largely as described previously
809 (Chen *et al.*, 2018). Aliquots of Met15 and Yll058w, purified as described above, were
810 dialyzed into a final storage buffer of 20 mM Tris-Cl pH 8.0, 500 mM NaCl, 20 mM
811 Imidazole, 0.2 mM pyridoxal 5'-phosphate (PLP), and 10% glycerol, snap frozen in
812 liquid N_2, and stored at -80°C. Aliquots were thawed on ice, and the enzymes were
813 diluted in the storage buffer to a concentration of 60 nM and preincubated at room

814 temperature for 10 minutes. The enzyme solution was then mixed with diluted 10x,
815 giving a final enzyme concentration of 6nM, with a reaction mixture containing 50 mM
816 Potassium phosphate buffer (pH 7.8), 1.0 mM EDTA pH 8.0, 15.0 mM O-acetyl-L-
817 homoserine, 5.0 mM NaHS, and 0.6 mM PLP. The reaction components were then
818 mixed by gentle pipetting and incubated at 30°C. Each reaction was performed in
819 triplicate. Samples were removed at 6 timepoints (0, 1, 3, 5, 10, and 15 minutes), and
820 the reactions were stopped by adding 1.0 M HCl at a ratio of 10mL for every 100mL of
821 sample, then snap frozen with liquid N_2. In the same buffer as the reaction mixture but
822 without any enzyme or substrate (but with acid added), we also generated a
823 homocysteine standard curve with seven serial 1:5 dilutions ranging from 15 mM to
824 0.00096 mM, as well as a 0 mM "blank" sample.
825
826 Ten µL of each enzyme reaction were extracted and derivatized with N-ethylmaleamide
827 (NEM**;** Alfa Aesar, Cat# 40526-06) in 990 µL of ice-cold extraction solvent (80% MeOH:
828 20% H_2O containing 25 mM NEM and 10 mM ammonium formate, pH=7.0) containing
829 0.5 uM of [D_4]-Homocysteine **(**Cambridge Isotope labs, Cat# DLM-8259-PK**)** followed by
830 incubation at 4°C for 30 min. After centrifugation (17,000 g, 20 min, 4°C), the
831 supernatants were analyzed by LC-MS following previously established conditions
832 (Kang et al., 2019). For the chromatographic metabolite separation, a Vanquish UPLC
833 system was coupled to a Q Exactive HF (QE-HF) mass spectrometer equipped with
834 HESI (Thermo Fisher Scientific, Waltham, MA). The column was a SeQuant ZIC-pHILIC
835 LC column, 5 mm, 150 x 4.6mm (MilliporeSigma, Burlington, MA) with a SeQuant ZIC-
836 pHILIC guard column, 20 x 4.6 mm (MilliporeSigma, Burlington, MA). Mobile phase A

837 was 10 mM $(NH_4)_2CO_3$ and 0.05% NH_4OH in H_2O while mobile phase B was 100%
838 ACN. The column chamber temperature was set to 30°C. The mobile phase condition
839 was set according to the following gradient: 0-13min: 80% to 20% of mobile phase B,
840 13-15min: 20% of mobile phase B. The ESI ionization mode was positive. The MS scan
841 range (m/z) was set to 60-900. The mass resolution was 120,000 and the AGC target
842 was 3 x 10^6. Capillary voltage and capillary temperature were set to 3.5 KV and 320°C,
843 respectively. Five µL of sample was loaded. The homocysteine and [D_4]-Homocysteine
844 peaks were manually identified and integrated with EL-Maven (Version 0.11.0) by
845 matching with an in-house library. Homocysteine levels were calculated using the
846 standard curve and corrected using the [D_4]-Homocysteine internal standard.
847

848 **Metabolic Modeling**

849 Metabolic modeling simulations were performed with Python script making use of the
850 COBRApy toolkit (Ebrahim et al., 2013) and the ecYeastGEM_batch model (Lu *et al.*,
851 2019), an "enzyme-constrained" variant (Sanchez et al., 2017) of Yeast8. The enzyme-
852 constrained feature of the steady-state model is achieved by treating enzymes as
853 metabolites that are temporarily "consumed" (i.e. removed from the available pool) while
854 they are engaged in catalysis. The script first removes all preexisting reactions (which
855 have not been experimentally validated) contributing to the "consumption" of Yll058w
856 (r_0815No1, r_0815REVNo1, and arm_r_0815). Second, the script adds the
857 hypothetical homocysteine-generating reaction that we observe in our *in vitro* assay,
858 which uses H_2S and *O*-acetylhomoserine as substrates and yields homocysteine,
859 acetate, and hydrogen as products, with Yll058w as the catalyst. This reaction was

860 added with a range of Kcat values assigned to Yll058w in order to evaluate the
861 "biomass" generated over a broad range of enzyme efficiencies. The reaction catalyzed
862 by Yll058w was made to be bidirectional; however, flux was only observed in the
863 forward (homocysteine-producing) reaction. Thirdly, *MET15* was removed from the
864 model, eliminating all reactions that the encoded enzyme was associated with. Finally,
865 the model was "solved" to obtain the flux through the biomass equation, a proxy for
866 fitness. The default growth medium associated with the model, which contains sulfates
867 but lacks organosulfurs, was used for all simulations.
868
869 **Chelation of H_2S with Ferric-EDTA sodium salt**
870 For each strain (FY4, FY4-*met15Δ*, and their respective petite derivatives), five single
871 colonies were scraped from a YPDA agar plate and cells were resuspended in SD-
872 Met+Glu medium. The optical density at 600 nm (OD_{600}) of the suspension was
873 measured using a spectrophotometer, and 25mL cultures were inoculated at a starting
874 OD_{600} of 0.1 in SD-Met+Glu or SD-Met+Glu supplemented with 0.048M Ferric (Fe)-
875 EDTA (Ethylenediaminetetraacetic acid ferric sodium salt, E6067, Millipore Sigma) in
876 125mL Erlenmeyer flasks (optimal Fe-EDTA dosage was determined by a titration
877 experiment (**Figure S11**)). For the non-petite strains, the experiment was performed
878 twice; each time, cultures were prepared in triplicate. The petite strains were tested in a
879 single experiment using four biological replicates. Cultures were incubated at 30°C with
880 150rpm shaking and OD_{600} was measured regularly until saturation was reached (~51 to
881 53 hours). For the repassaging of the non-petite strains (**Figure 4A-C**), cells were then
882 pelleted to facilitate the exchange to fresh SD-Met+Glu medium, again using a starting

883 OD_{600} of 0.1, and incubated as before for ~51 hours with regular OD_{600} measurements.
884 A portion of each culture was stored at 4°C. Ten μl drops of each culture (both the
885 original culture and after the repassaged growth) were then both spotted and struck on
886 agar plates (YPDA, SD-Met+Glu, SC-Met-Cys+Glu, SC-Met-Cys+Glu+(Fe-EDTA) and
887 BiGGY) that were incubated at 30°C (**Figure 4C**) and imaged regularly with spImager
888 Automated Imaging System (S & P Robotics Inc., Ontario, Canada). All experiments
889 carried out in liquid media are indicated with a gray background.
890
891 **Data availability**
892 All data generated/analyzed in this study are available in the main text, in the
893 Supplementary Figures and Tables, and as Supplementary Data files. Supplementary
894 material is available at https://bit.ly/3GIgpld.
895
896 **Code availability**
897 All images and statistical analyses in this study were generated using code available at
898 https://github.com/sauriiiin/methionine/tree/master/paper.
899
900
901

902 **ACKNOWLEDGEMENTS**

903 We thank all the members of the Carvunis Lab, and in particular Carly Houghton, for
904 helpful suggestions during lab meetings and presentations. We also thank Kate
905 Metedgul-Ernar, Cameron Hines and Brian Hsu for their precious help in the early
906 stages of the project and S.G. Wendell and Steven Mullett for their assistance with
907 mass spectrometry analysis.

908

909 **FUNDING**

910 This work was supported by the National Institutes of Health grant R00GM108865 to A.-
911 R.C, F32GM129929 to S.B.V.O, P01CA250984 to G.M.D, NIHS10OD023402 to S.G.W.,
912 and the AACR-Takeda Oncology Lung Cancer Research Fellowship (19-40-38-KANG)
913 to Y.P.K.

914

915 **AUTHOR CONTRIBUTIONS**

916 Conceptualization: S.B.V.O., S.B.P., N.C.C., G.M.D., A-R.C. Methodology: S.B.V.O.,
917 S.B.P., N.C.C., A.W., A.P.V., G.M.D., A-R.C. Investigation: S.B.V.O., S.B.P., N.C.C.,
918 A.W., I.B., M.M., J.X., Y.P.K., K.M.M., J.M., A.P.V. Writing: S.B.V.O., S.B.P., N.C.C.,
919 A.W., A-R.C. Review and Editing: S.B.V.O., S.B.P., N.C.C., T.I., A.P.V., G.M.D., A-R.C.
920 Supervision: A-R.C.

921

922 **DECLARATION OF INTERESTS**

923 A.-R. C. is a member of the scientific advisory board for Flagship Labs 69, Inc. T.I. is a
924 co-founder of Data4Cure and has an equity interest. T.I. is on the Scientific Advisory

Board of Ideaya BioSciences, Inc., has an equity interest, and receives income. The terms of these arrangements have been reviewed and approved by the University of California San Diego in accordance with its conflict of interest policies.

928 **REFERENCES**

929

930 Bean, G.J., Jaeger, P.A., Bahr, S., and Ideker, T. (2014). Development of ultra-high-
931 density screening tools for microbial "omics". PLoS One *9*, e85177.
932 10.1371/journal.pone.0085177.
933 Blackstone, E., Morrison, M., and Roth, M.B. (2005). H2S induces a suspended
934 animation-like state in mice. Science *308*, 518. 10.1126/science.1108581.
935 Boeke Lab (2003). The Met15 Resource: Update.
936 http://www.bs.jhmi.edu/mbg/boekelab/Resources/Met15/Met15updt.html.
937 Boer, V.M., Amini, S., and Botstein, D. (2008). Influence of genotype and nutrition on
938 survival and metabolism of starving yeast. Proc Natl Acad Sci U S A *105*, 6930-6935.
939 10.1073/pnas.0802601105.
940 Brachmann, C.B., Davies, A., Cost, G.J., Caputo, E., Li, J., Hieter, P., and Boeke, J.D.
941 (1998). Designer deletion strains derived from Saccharomyces cerevisiae S288C: a
942 useful set of strains and plasmids for PCR-mediated gene disruption and other
943 applications. Yeast *14*, 115-132. 10.1002/(SICI)1097-0061(19980130)14:2<115::AID-
944 YEA204>3.0.CO;2-2.
945 Brewster, J.L., Pachl, P., McKellar, J.L.O., Selmer, M., Squire, C.J., and Patrick, W.M.
946 (2021). Structures and kinetics of Thermotoga maritima MetY reveal new insights into
947 the predominant sulfurylation enzyme of bacterial methionine biosynthesis. J Biol Chem
948 *296*, 100797. 10.1016/j.jbc.2021.100797.

949 Byrne, K.P., and Wolfe, K.H. (2005). The Yeast Gene Order Browser: combining
950 curated homology and syntenic context reveals gene fate in polyploid species. Genome
951 Res *15*, 1456-1461. 10.1101/gr.3672305.
952 Chen, Z., Zhang, X., Li, H., Liu, H., Xia, Y., and Xun, L. (2018). The Complete Pathway
953 for Thiosulfate Utilization in Saccharomyces cerevisiae. Appl Environ Microbiol *84*.
954 10.1128/AEM.01241-18.
955 DiCarlo, J.E., Norville, J.E., Mali, P., Rios, X., Aach, J., and Church, G.M. (2013).
956 Genome engineering in Saccharomyces cerevisiae using CRISPR-Cas systems.
957 Nucleic Acids Res *41*, 4336-4343. 10.1093/nar/gkt135.
958 Douglas, A.C., Smith, A.M., Sharifpoor, S., Yan, Z., Durbic, T., Heisler, L.E., Lee, A.Y.,
959 Ryan, O., Gottert, H., Surendra, A., et al. (2012). Functional analysis with a barcoder
960 yeast gene overexpression system. G3 (Bethesda) *2*, 1279-1289.
961 10.1534/g3.112.003400.
962 Dunham, M.J., Gartenberg, M. R., Brown, G. W. (2015). Methods in Yeast Genetics and
963 Genomics, 2015 Edition: A CSHL Course Manual (Cold Spring Harbor Laboratory
964 Press).
965 Ebrahim, A., Lerman, J.A., Palsson, B.O., and Hyduke, D.R. (2013). COBRApy:
966 COnstraints-Based Reconstruction and Analysis for Python. BMC Syst Biol *7*, 74.
967 10.1186/1752-0509-7-74.
968 Eddy, S.R. (2011). Accelerated Profile HMM Searches. PLoS Comput Biol *7*, e1002195.
969 10.1371/journal.pcbi.1002195.
970 Endicott, M., Jones, M., and Hull, J. (2021). Amino acid metabolism as a therapeutic
971 target in cancer: a review. Amino Acids *53*, 1169-1179. 10.1007/s00726-021-03052-1.

Ferguson, L.R., and von Borstel, R.C. (1992). Induction of the cytoplasmic 'petite' mutation by chemical and physical agents in Saccharomyces cerevisiae. Mutat Res *265*, 103-148. 10.1016/0027-5107(92)90042-z.

Gaensly, F., Picheth, G., Brand, D., and Bonfim, T.M. (2014). The uptake of different iron salts by the yeast Saccharomyces cerevisiae. Braz J Microbiol *45*, 491-494. 10.1590/s1517-83822014000200016.

Giaever, G., and Nislow, C. (2014). The yeast deletion collection: a decade of functional genomics. Genetics *197*, 451-465. 10.1534/genetics.114.161620.

Green, C.L., Lamming, D.W., and Fontana, L. (2021). Molecular mechanisms of dietary restriction promoting health and longevity. Nat Rev Mol Cell Biol. 10.1038/s41580-021-00411-4.

Hansen, J., and Johannesen, P.F. (2000). Cysteine is essential for transcriptional regulation of the sulfur assimilation genes in Saccharomyces cerevisiae. Mol Gen Genet *263*, 535-542. 10.1007/s004380051199.

Hou, J., van Leeuwen, J., Andrews, B.J., and Boone, C. (2018). Genetic Network Complexity Shapes Background-Dependent Phenotypic Expression. Trends Genet *34*, 578-586. 10.1016/j.tig.2018.05.006.

Johnson, J.E., and Johnson, F.B. (2014). Methionine restriction activates the retrograde response and confers both stress tolerance and lifespan extension to yeast, mouse and human cells. PLoS One *9*, e97729. 10.1371/journal.pone.0097729.

Jumper, J., Evans, R., Pritzel, A., Green, T., Figurnov, M., Ronneberger, O., Tunyasuvunakool, K., Bates, R., Zidek, A., Potapenko, A., et al. (2021). Highly accurate

994 protein structure prediction with AlphaFold. Nature *596*, 583-589. 10.1038/s41586-021-
995 03819-2.
996 Kang, Y.P., Torrente, L., Falzone, A., Elkins, C.M., Liu, M., Asara, J.M., Dibble, C.C.,
997 and DeNicola, G.M. (2019). Cysteine dioxygenase 1 is a metabolic liability for non-small
998 cell lung cancer. Elife *8*, e45572.
999 Laxman, S., Sutter, B.M., Wu, X., Kumar, S., Guo, X., Trudgian, D.C., Mirzaei, H., and
1000 Tu, B.P. (2013). Sulfur amino acids regulate translational capacity and metabolic
1001 homeostasis through modulation of tRNA thiolation. Cell *154*, 416-429.
1002 10.1016/j.cell.2013.06.043.
1003 Lee, T.A., Jorgensen, P., Bognar, A.L., Peyraud, C., Thomas, D., and Tyers, M. (2010).
1004 Dissection of combinatorial control by the Met4 transcriptional complex. Mol Biol Cell
1005 *21*, 456-469. 10.1091/mbc.E09-05-0420.
1006 Linderholm, A.L., Findleton, C.L., Kumar, G., Hong, Y., and Bisson, L.F. (2008).
1007 Identification of genes affecting hydrogen sulfide formation in Saccharomyces
1008 cerevisiae. Appl Environ Microbiol *74*, 1418-1427. 10.1128/AEM.01758-07.
1009 Lu, H., Li, F., Sanchez, B.J., Zhu, Z., Li, G., Domenzain, I., Marcisauskas, S., Anton,
1010 P.M., Lappa, D., Lieven, C., et al. (2019). A consensus S. cerevisiae metabolic model
1011 Yeast8 and its ecosystem for comprehensively probing cellular metabolism. Nat
1012 Commun *10*, 3586. 10.1038/s41467-019-11581-3.
1013 Madeira, F., Park, Y.M., Lee, J., Buso, N., Gur, T., Madhusoodanan, N., Basutkar, P.,
1014 Tivey, A.R.N., Potter, S.C., Finn, R.D., and Lopez, R. (2019). The EMBL-EBI search
1015 and sequence analysis tools APIs in 2019. Nucleic Acids Res *47*, W636-W641.
1016 10.1093/nar/gkz268.

1017 Masselot, M., and De Robichon-Szulmajster, H. (1975). Methionine biosynthesis in
1018 Saccharomyces cerevisiae. I. Genetical analysis of auxotrophic mutants. Mol Gen
1019 Genet *139*, 121-132. 10.1007/BF00264692.
1020 Nickerson, W.J. (1953). Reduction of inorganic substances by yeasts. I. Extracellular
1021 reduction of sulfite by species of Candida. J Infect Dis *93*, 43-56. 10.1093/infdis/93.1.43.
1022 Ono, B., Shirahige, Y., Nanjoh, A., Andou, N., Ohue, H., and Ishino-Arao, Y. (1988).
1023 Cysteine biosynthesis in Saccharomyces cerevisiae: mutation that confers cystathionine
1024 beta-synthase deficiency. J Bacteriol *170*, 5883-5889. 10.1128/jb.170.12.5883-
1025 5889.1988.
1026 Parikh, S.B., Castilho Coelho, N., and Carvunis, A.R. (2021). LI Detector: a framework
1027 for sensitive colony-based screens regardless of the distribution of fitness effects. G3
1028 (Bethesda) *11*. 10.1093/g3journal/jkaa068.
1029 Paul, B.D., Snyder, S.H., and Kashfi, K. (2021). Effects of hydrogen sulfide on
1030 mitochondrial function and cellular bioenergetics. Redox Biol *38*, 101772.
1031 10.1016/j.redox.2020.101772.
1032 Philip, C.V., and Brooks, D.W. (1974). Iron(III) chelate complexes of hydrogen sulfide
1033 and mercaptans in aqueous solution. Inorganic Chemistry *13*, 384-386.
1034 10.1021/ic50132a030.
1035 Plummer, J.D., and Johnson, J.E. (2019). Extension of Cellular Lifespan by Methionine
1036 Restriction Involves Alterations in Central Carbon Metabolism and Is Mitophagy-
1037 Dependent. Front Cell Dev Biol *7*, 301. 10.3389/fcell.2019.00301.

1038 Raymond, R.K., Kastanos, E.K., and Appling, D.R. (1999). Saccharomyces cerevisiae
1039 expresses two genes encoding isozymes of methylenetetrahydrofolate reductase. Arch
1040 Biochem Biophys *372*, 300-308. 10.1006/abbi.1999.1498.
1041 Ruckenstuhl, C., Netzberger, C., Entfellner, I., Carmona-Gutierrez, D., Kickenweiz, T.,
1042 Stekovic, S., Gleixner, C., Schmid, C., Klug, L., Sorgo, A.G., et al. (2014). Lifespan
1043 extension by methionine restriction requires autophagy-dependent vacuolar
1044 acidification. PLoS Genet *10*, e1004347. 10.1371/journal.pgen.1004347.
1045 Ryan, O.W., Skerker, J.M., Maurer, M.J., Li, X., Tsai, J.C., Poddar, S., Lee, M.E.,
1046 DeLoache, W., Dueber, J.E., Arkin, A.P., and Cate, J.H. (2014). Selection of
1047 chromosomal DNA libraries using a multiplex CRISPR system. Elife *3*.
1048 10.7554/eLife.03703.
1049 Sanchez, B.J., Zhang, C., Nilsson, A., Lahtvee, P.J., Kerkhoven, E.J., and Nielsen, J.
1050 (2017). Improving the phenotype predictions of a yeast genome-scale metabolic model
1051 by incorporating enzymatic constraints. Mol Syst Biol *13*, 935. 10.15252/msb.20167411.
1052 Shen, X.X., Opulente, D.A., Kominek, J., Zhou, X., Steenwyk, J.L., Buh, K.V., Haase,
1053 M.A.B., Wisecaver, J.H., Wang, M., Doering, D.T., et al. (2018). Tempo and Mode of
1054 Genome Evolution in the Budding Yeast Subphylum. Cell *175*, 1533-1545 e1520.
1055 10.1016/j.cell.2018.10.023.
1056 Singh, A., and Sherman, F. (1974). Association of methionine requirement with methyl
1057 mercury resistant mutants of yeast. Nature *247*, 227-229. 10.1038/247227a0.
1058 Sprouffske, K., and Wagner, A. (2016). Growthcurver: an R package for obtaining
1059 interpretable metrics from microbial growth curves. BMC Bioinformatics *17*, 172.
1060 10.1186/s12859-016-1016-7.

1061 Stanford University (2020). Saccharomyces Genome Database.
1062 https://www.yeastgenome.org/.
1063 Sutter, B.M., Wu, X., Laxman, S., and Tu, B.P. (2013). Methionine inhibits autophagy
1064 and promotes growth by inducing the SAM-responsive methylation of PP2A. Cell *154*,
1065 403-415. 10.1016/j.cell.2013.06.041.
1066 Team, R.C. (2021). R: A language and environment for statistical computing. (R
1067 Foundation for Statistical Computing, Vienna, Austria.).
1068 Thomas, D., and Surdin-Kerjan, Y. (1997). Metabolism of sulfur amino acids in
1069 Saccharomyces cerevisiae. Microbiol Mol Biol Rev *61*, 503-532.
1070 Van Oss, S.B., Shirra, M.K., Bataille, A.R., Wier, A.D., Yen, K., Vinayachandran, V.,
1071 Byeon, I.L., Cucinotta, C.E., Heroux, A., Jeon, J., et al. (2016). The Histone Modification
1072 Domain of Paf1 Complex Subunit Rtf1 Directly Stimulates H2B Ubiquitylation through
1073 an Interaction with Rad6. Mol Cell *64*, 815-825. 10.1016/j.molcel.2016.10.008.
1074 Vowinckel, J., Hartl, J., Marx, H., Kerick, M., Runggatscher, K., Keller, M.A., Mulleder,
1075 M., Day, J., Weber, M., Rinnerthaler, M., et al. (2021). The metabolic growth limitations
1076 of petite cells lacking the mitochondrial genome. Nat Metab *3*, 1521-1535.
1077 10.1038/s42255-021-00477-6.
1078 Walvekar, A.S., and Laxman, S. (2019). Methionine at the Heart of Anabolism and
1079 Signaling: Perspectives From Budding Yeast. Front Microbiol *10*, 2624.
1080 10.3389/fmicb.2019.02624.
1081 Wang, H., Robinson, J.L., Kocabas, P., Gustafsson, J., Anton, M., Cholley, P.E., Huang,
1082 S., Gobom, J., Svensson, T., Uhlen, M., et al. (2021). Genome-scale metabolic network

1083 reconstruction of model animals as a platform for translational research. Proc Natl Acad
1084 Sci U S A *118*. 10.1073/pnas.2102344118.
1085 Wilson, D., Pethica, R., Zhou, Y., Talbot, C., Vogel, C., Madera, M., Chothia, C., and
1086 Gough, J. (2009). SUPERFAMILY--sophisticated comparative genomics, data mining,
1087 visualization and phylogeny. Nucleic Acids Res *37*, D380-386. 10.1093/nar/gkn762.
1088 Winston, F., Dollard, C., and Ricupero-Hovasse, S.L. (1995). Construction of a set of
1089 convenient Saccharomyces cerevisiae strains that are isogenic to S288C. Yeast *11*, 53-
1090 55. 10.1002/yea.320110107.
1091 Yamagata, S. (1971). Homocysteine synthesis in yeast. Partial purification and
1092 properties of O-acetylhomoserine sulfhydrylase. J Biochem *70*, 1035-1045.
1093 10.1093/oxfordjournals.jbchem.a129712.
1094 Yamagata, S. (1976). O-Acetylserine and O-acetylhomoserine sulfhydrylase of yeast.
1095 Subunit structure. J Biochem *80*, 787-797. 10.1093/oxfordjournals.jbchem.a131339.
1096 Zhang, Z., and Ren, Q. (2015). Why are essential genes essential? - The essentiality of
1097 Saccharomyces genes. Microb Cell *2*, 280-287. 10.15698/mic2015.08.218.
1098 Zou, K., Ouyang, Q., Li, H., and Zheng, J. (2017). A global characterization of the
1099 translational and transcriptional programs induced by methionine restriction through
1100 ribosome profiling and RNA-seq. BMC Genomics *18*, 189. 10.1186/s12864-017-3483-2.
1101

SUPPLEMENTARY MATERIAL

SUPPLEMENTARY FIGURES

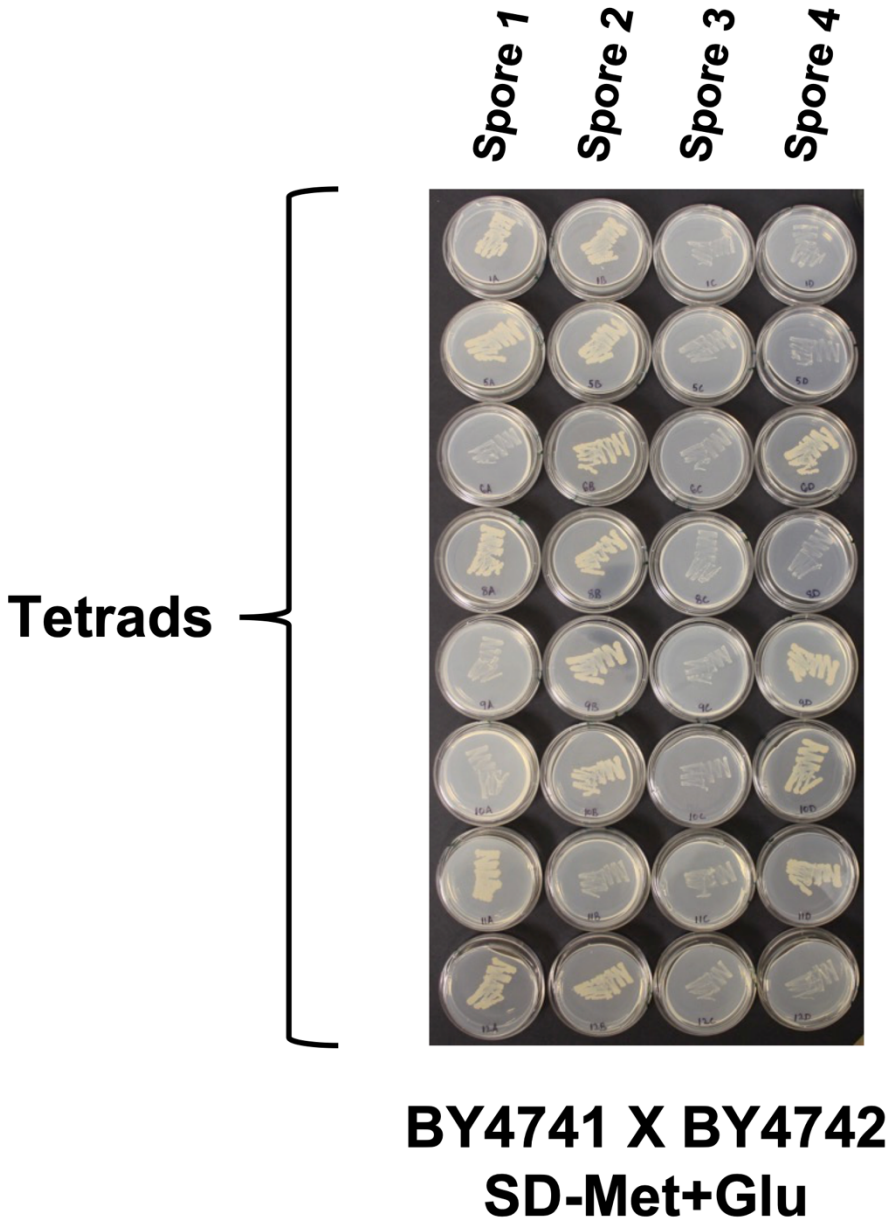

Figure S1. *met15Δ*-associated growth phenotype segregates 2:2 in a heterozygous cross. The BY4741 and BY4742 strains were mated, sporulated, and dissected using standard techniques. Eight four-spore tetrads were grown on YPDA, and then patched onto SD-Met+Glu medium. Individual plates were used to prevent cross-feeding between *MET15*$^{+}$ and *met15Δ* cells. Each tetrad resulted in 2:2 segregation of the growth phenotype on organosulfur-deficient media. Notably, the growth of *met15Δ* thick patches was substantially weaker than that observed in the automated colony transfer assays used throughout the manuscript.

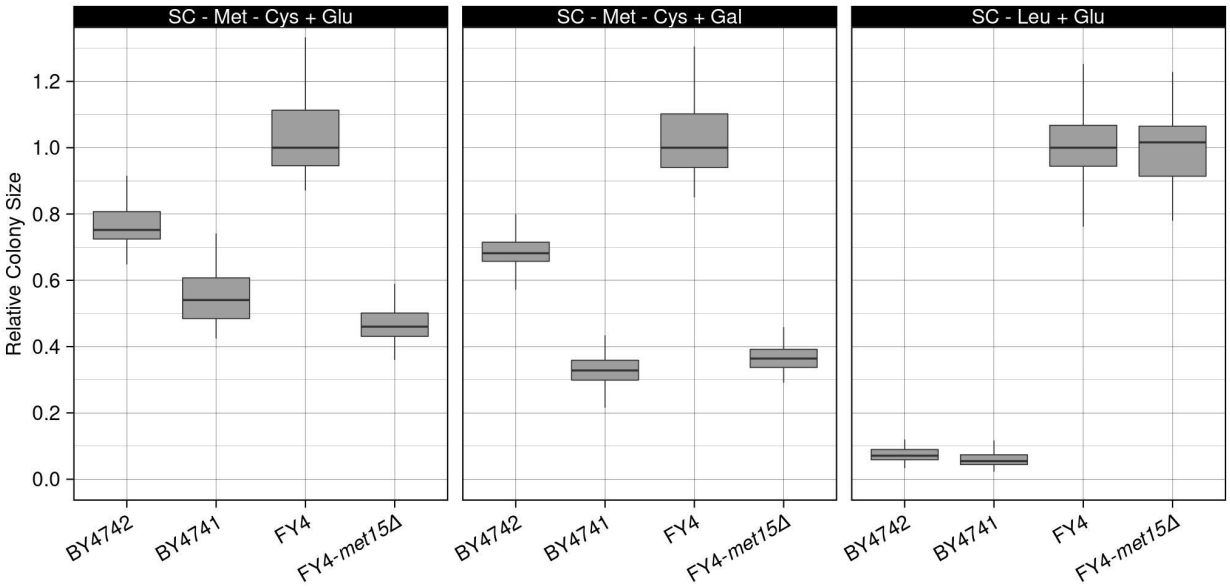

Figure S2. *met15Δ* cells also grow robustly in "synthetic complete" (SC) media lacking organosulfurs. The same automated colony transfer and analysis pipeline shown in **Figure 1A-C** was repeated, here on SC-Met-Cys media containing either glucose or galactose as the sole carbon source, or on SC-Leu+Glu medium, where the negligible growth of the BY4741 and BY4742 strains is consistent with auxotrophy. The prototrophic strain FY4 and a mutant derivative lacking *MET15* were also assayed. Box plots represent relative colony sizes (y-axis) at saturation (~140 hours (SC-Leu+Glu) or 165 hours (SC-Met+Glu/Gal)) of BY4742, BY4741, FY4 and FY4-*met15Δ* (x-axis). Relative colony size is normalized to the mean colony size of FY4 grown in the same condition (see **Materials and Methods**).

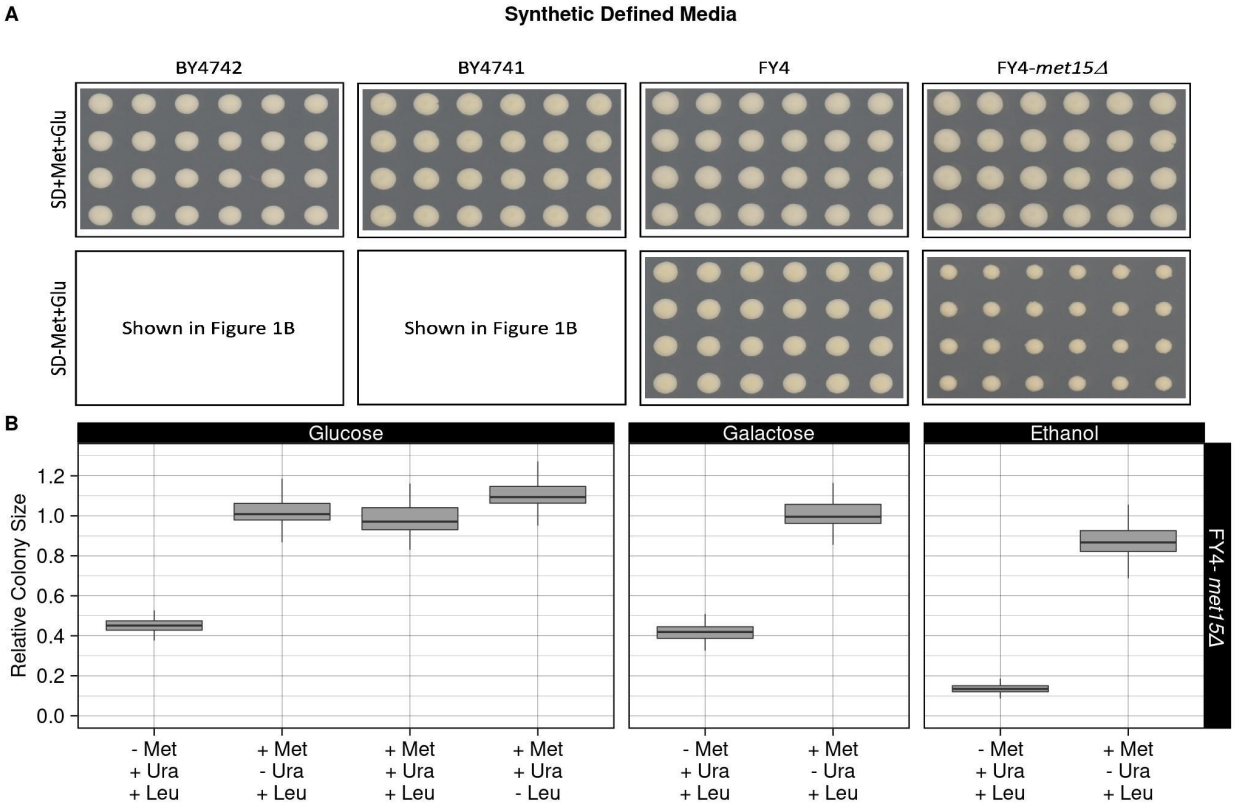

Figure S3. Robust growth of *met15Δ* cells in an organosulfur-deficient medium. A) In "synthetic defined" medium lacking methionine and with glucose comprising the carbon source (SD-Met+Glu), cells harboring the *met15Δ0* deletion (BY4741) or a "scarless deletion" of *MET15* made by CRISPR (FY4-*met15Δ*) show surprisingly robust growth inconsistent with their presumed auxotrophy, while in "conventional" SD medium (SD+Met+Glu), these mutant cells form slightly larger colonies than their nearly isogenic *MET15*$^{+}$ counterparts, BY4741 and FY4, respectively. Colonies shown here have grown for 366 hours. Related to **Figure 1B**. **B)** The "scarless" CRISPR *met15Δ* mutant shows similarly robust growth, inconsistent with auxotrophy, when glucose or galactose comprise the carbon source, but growth is much weaker when the same strain is grown with ethanol as the carbon source. Box plots represent relative colony sizes (y-axis) at saturation (~358 to 366 hours). Relative colony size is normalized to the mean colony size of FY4 grown in the same condition (see **Materials and Methods**).

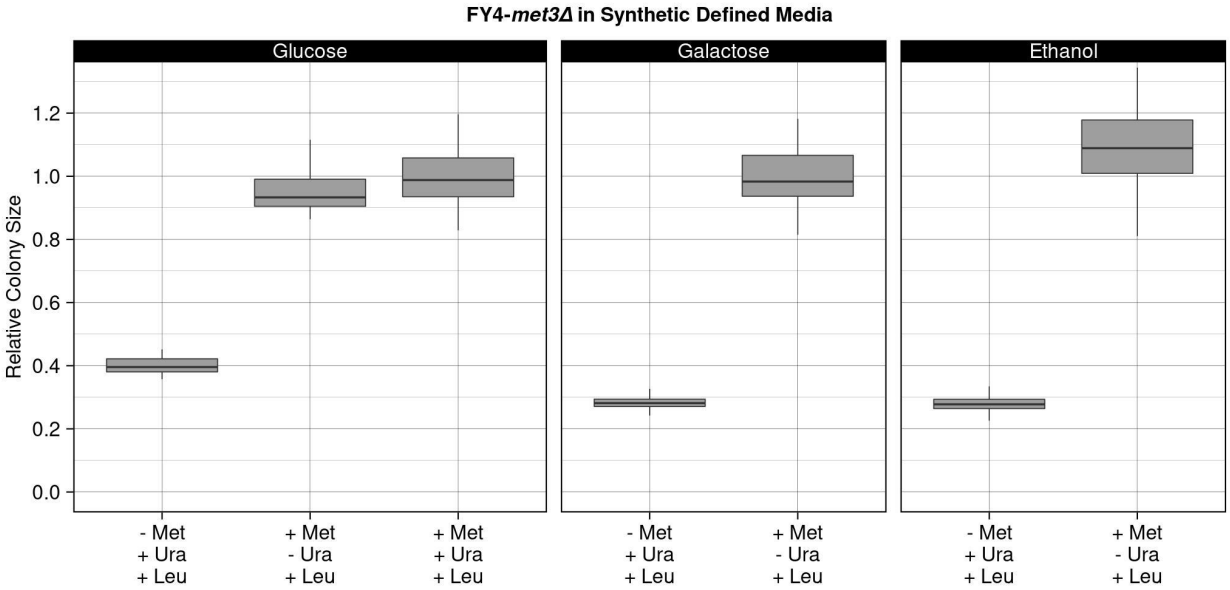

Figure S4. The growth of FY4-*met3Δ* cells on SD-Met media is generally unaffected by the carbon source. The FY4-*met3Δ* mutant was grown in the same manner as the strains presented in **Figures 1C** and **S3A-B**. Box plots represent relative colony sizes (y-axis) at saturation (366 hours). Relative colony size is normalized to the mean colony size of FY4 grown in the same condition (see **Materials and Methods**).

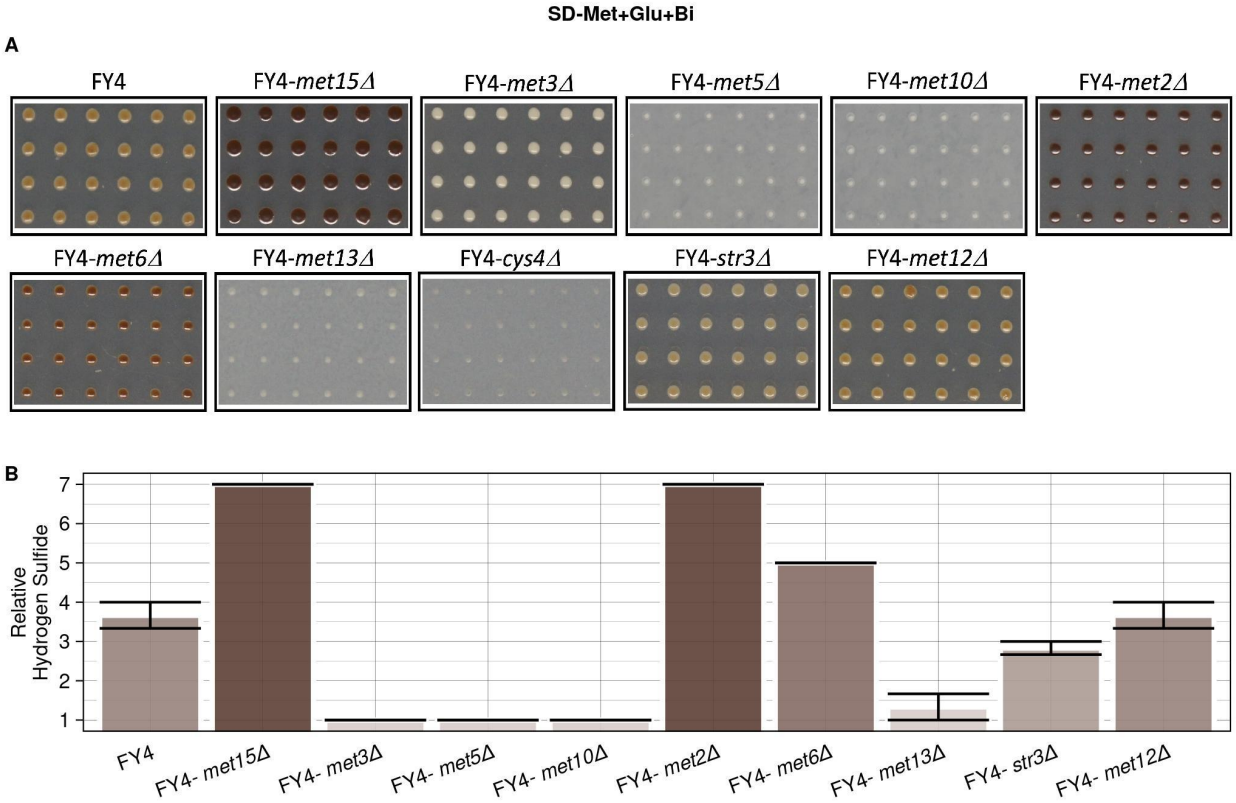

Figure S5. H_2S levels of mutant strains in an organosulfur-free medium. Cropped images (**Panel A**) and qualitative assessment of colony color (**Panel B**, performed in the same manner described in **Figure 2D**) of the mutant strains tested in **Figures 2C-D and S8B-C** pinned to SD-Met+Glu medium containing bismuth (SD-Met+Glu+Bi). The FY4-*cys4Δ* mutant showed no observable growth hence has been excluded from Panel B. The darkness of the colonies is a proxy for the level of excess H_2S in each strain.

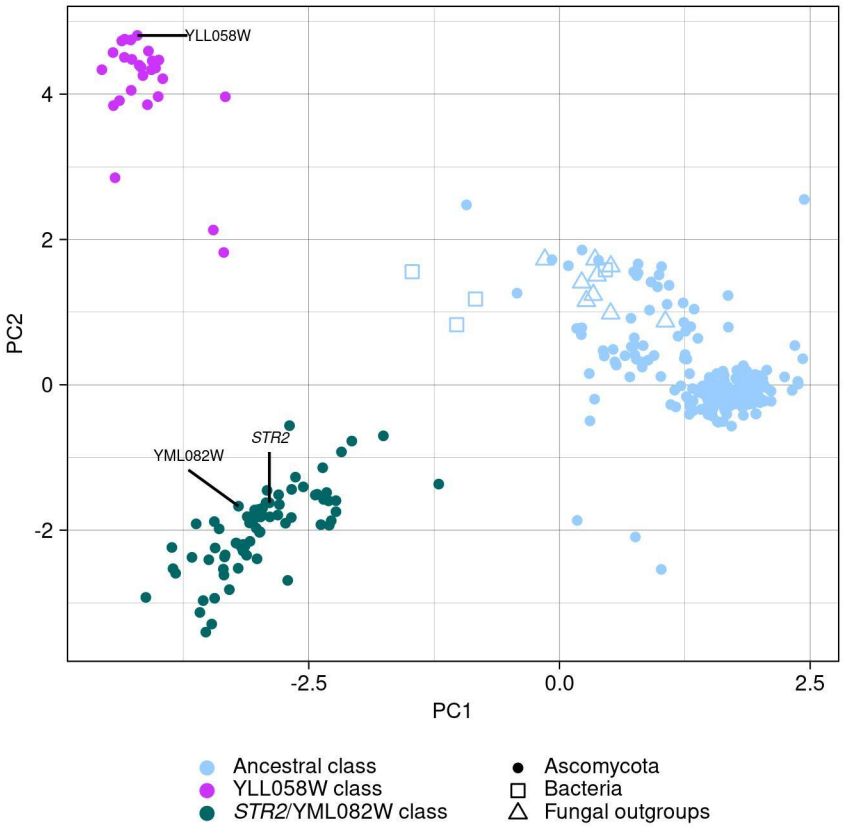

Figure S6. YLL058W homologs cluster into three distinct classes. Related to Figure 3B. The sequence distances between YLL058W homologs found in budding yeasts and outgroup taxa are visualized using multidimensional scaling (MDS). Points are colored according to k-means clustering based on these sequence distances using three clusters. The three genes contained in the *S. cerevisiae* genome are labeled.

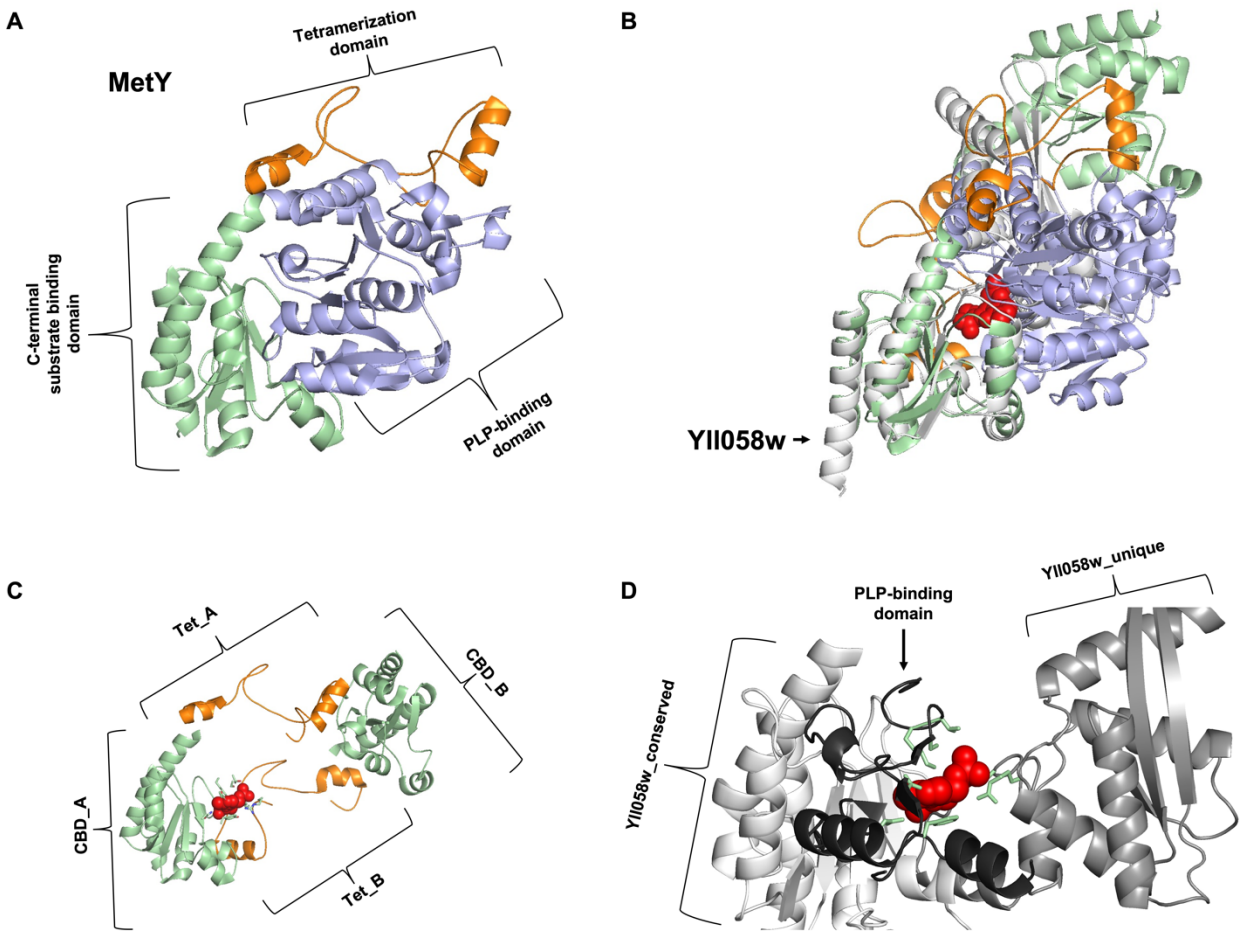

Figure S7. Yll058w functions as a monomer, in contrast to the tetrameric conformation seen in canonical homocysteine synthases. Related to Figure 3C. A) A cartoon view of the MetY monomer, from the MetY crystal structure, pdbID:7KB1 (Brewster et al., 2021). The N-terminal tetramerization domain is shown in orange, the PLP-binding domain is shown in light purple, and the C-terminal substrate binding domain is shown in pale green. **B)** The predicted structure of the monomeric Yll058w (white) is highly similar structurally to MetY within the PLP-binding and C-terminal domains and aligns well with a MetY dimer (reaction intermediate colored red for clarity). The Yll058w unique domain (Panel D), which replaces the tetramerization domain found in MetY, mimics part of the neigboring subunit from the MetY dimer, effectively preventing Yll058w from multimerizing in a manner similar to MetY. **C)** Cartoon view of the MetY N-terminal tetramerization domains (Tet_A and Tet_B; orange) and the C-terminal substrate binding domains (CBD_A, CBD_B; pale green) in contact with the reaction intermediate (red). The PLP-binding domains are hidden. Met15 (not shown) is predicted to adopt a similar conformation. **D)** The unique portion of the Yll058w monomer supplies the additional catalytic residues (pale green) provided by the second subunit of the MetY dimer. The portion of the predicted structure of Yll058w in contact with the reaction intermediate (red) is shown, with areas showing sequence and predicted structural similarity shown in white, and the region lacking homology to MetY and Met15 (Yll058w_unique) shown in gray. This unique region supports the possibility of Yll058w catalysis as a monomer, as opposed the confirmed (MetY) and predicted (Met15) multimeric structures of other homocysteine synthases. Portions of the PLP-binding domain that contribute putative catalytic residues are shown in black.

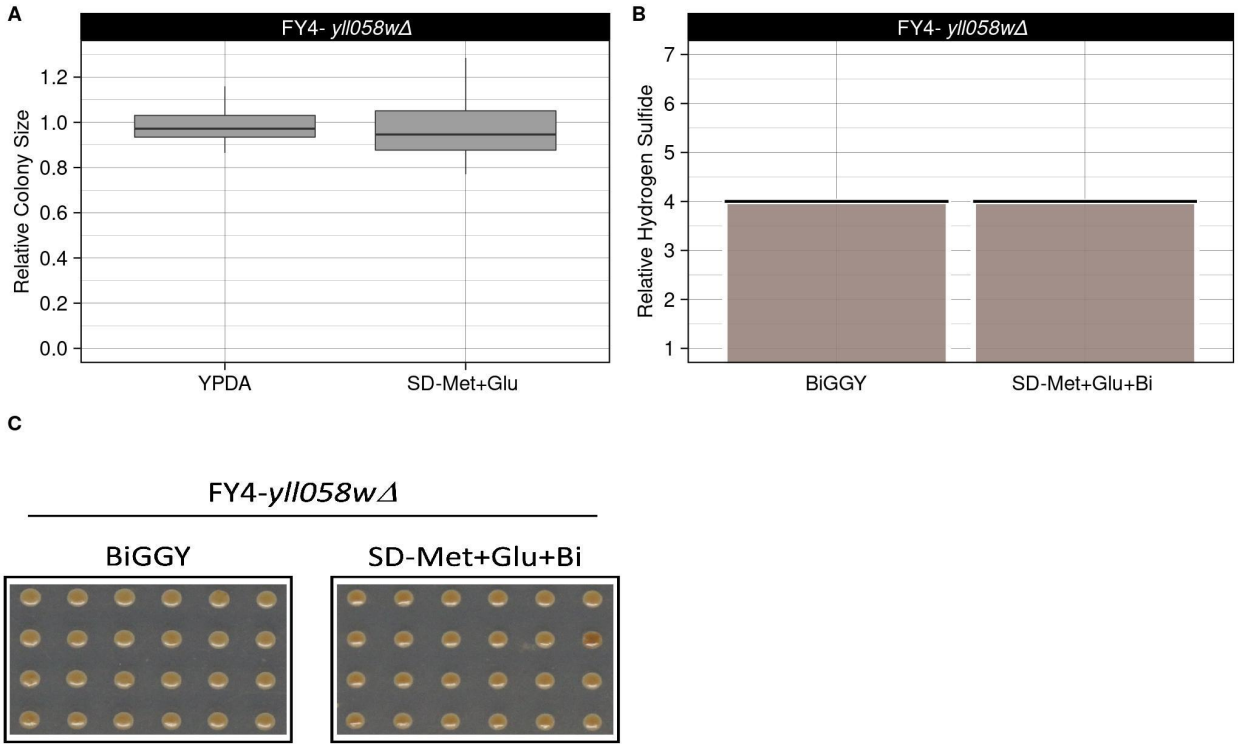

Figure S8. Deletion of YLL058W has negligible effect on fitness and H_2S accumulation in the FY4 background. Related to Figure 3D. A) Deletion of YLL058W in the prototrophic FY4 background has a negligible effect on growth in SD-Met+Glu medium. The strains were examined in the same manner as the mutants shown in **Figure 2B**, with colony size normalized to that of FY4**. B and C)** The relative H_2S level of FY4-*yll058wΔ*, as determined by growth on BiGGY and SD-Met+Glu+Bi, is comparable to that of wild-type FY4 cells. For Panel B, the darkness of the colonies was scored on the same qualitative scale applied to the mutants in **Figures 2C-D and S5B**.

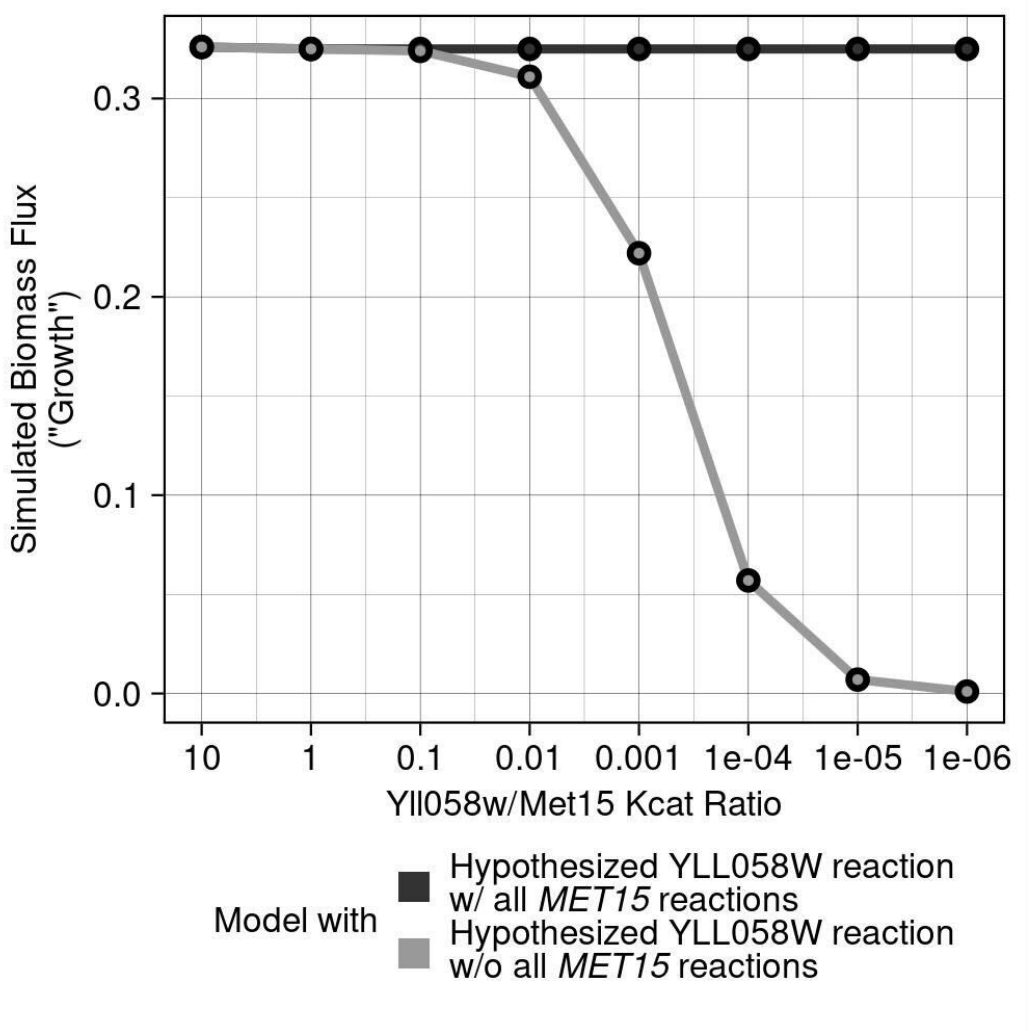

Figure S9. Simulated growth utilizing the consensus, genome-scale *S. cerevisiae* metabolic model (Lu et al., 2019) shows that a low-efficiency homocysteine synthase can support growth. Growth in an organosulfur-free medium is predicted *in silico* even with a homocysteine synthase with a dramatically lower catalytic efficiency than Met15. Two modifications were made to the default model – the addition of the *in vitro* reaction carried out in **Figure 3E** utilizing Yll058w as the catalytic enzyme (black), and the subsequent removal of the *MET15* gene from the model (gray). The y-axis indicates the flux through the "biomass equation", a proxy for growth/fitness, and the x-axis indicates different catalytic efficiency (Kcat) values assigned to Yll058w, relative to the default Kcat assigned to Met15, with the efficiency of Yll058w in the hypothetical reaction decreasing from left to right.

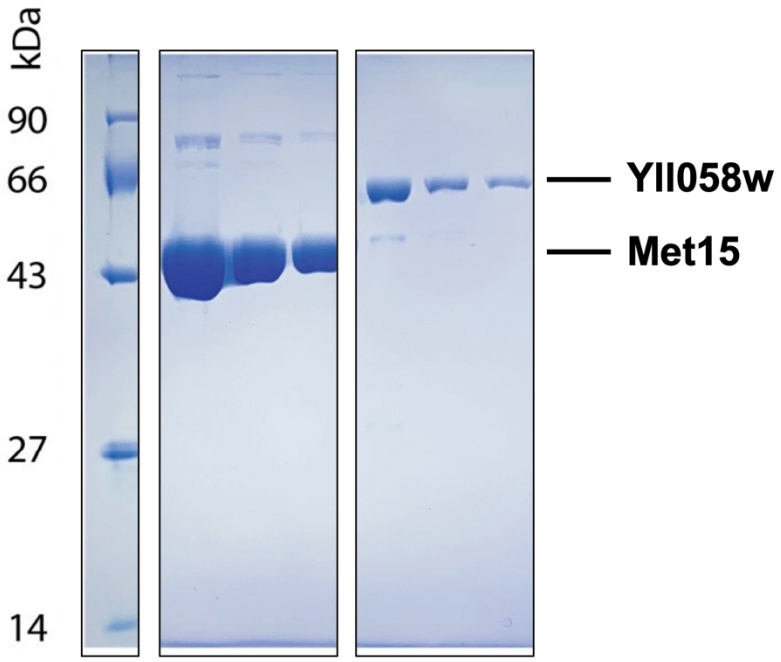

Figure S10. Coomassie-stained SDS-PAGE gel showing the final fractions that contained the recombinantly-expressed, purified protein used in the *in vitro* homocysteine biosynthesis assay. A lane containing molecular weight standards (kDa = kilodaltons) is shown on the left. Lanes containing less pure fractions that were not used were cropped, but the image is otherwise unaltered.

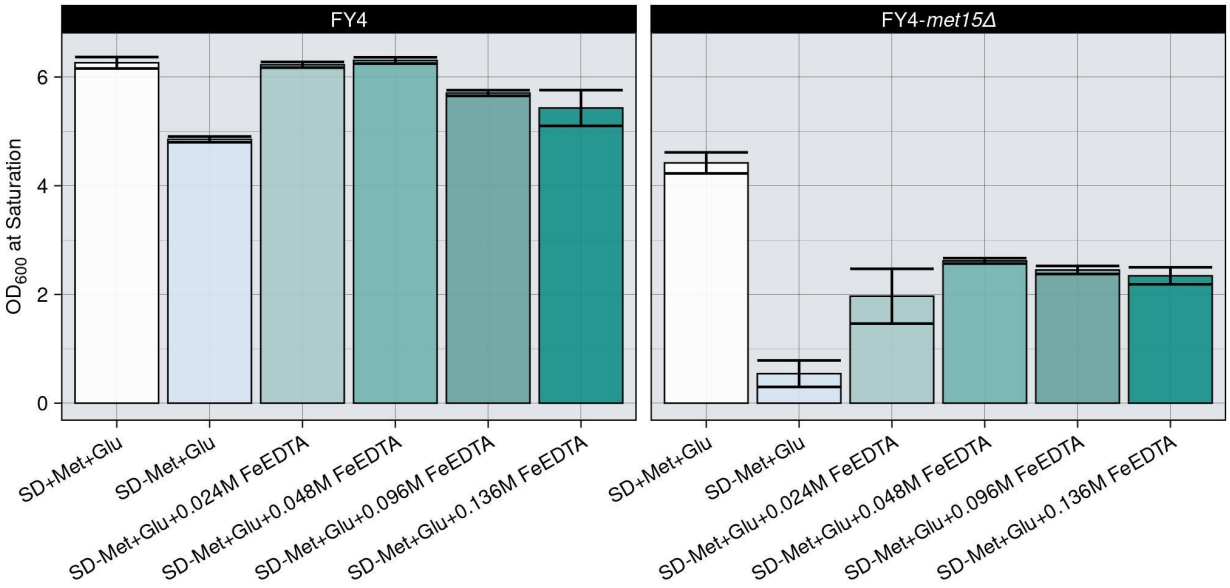

Figure S11. Titration of the H_2S chelator Fe-EDTA. Related to Figure 4. To determine the optimal dosage of Fe-EDTA for the experiments depicted in **Figures 4B-D**, FY4 and FY4-met15*Δ* cultures were grown in SD+Met+Glu and SD-Met+Glu supplemented with Fe-EDTA, with concentrations raging from 0 to 0.136 M. The concentration of 0.048 M yielded the greatest restoration of growth in FY4-met15*Δ* cultures. Bar plot: mean OD_{600}. Error bars: standard error.

SUPPLEMENTARY TABLES

Table S1. Settings for the RoToR HDA robotic plate handler used for all of the automated pinning experiments described in the manuscript. Screening of the deletion collection involved all five unique settings, while the remaining pinning experiments all followed the general schema described in **Figure 1B** and used only the "384 Glycerol to 384 Plate" and "384 Plate to 384 Plate" settings.

SETTINGS					384 Glycerol to 384 Plate	384 Plate to 384 Plate
Source					384 MTP	384 Agar
Target					384 Agar	384 Agar
Pads					384 Long Pin	384 Short
Program					Spot Many	Replicate
	General					
		Quantity			2	N/A
		Recycle			None	None
		Plate Protection			Uncheck	Uncheck
		Pairs				
		Start Pair				
	Source					
		Offset				Automatic
			Max Radius			0.4 mm
		Offsets...				
		Pinning				
			Pin Pressure			32%
			Speed		19 mm per sec	19 mm per sec
			Backoff		0.5 mm	2 mm
			Repeat Pin		1 times	1 times
		Dry Mix				
			Clearance			0.5 mm
			Diameter			1 mm
			Cycles			1 rotations
		Wet Mix				
			Diameter		1 mm	
			Speed		25 mm per sec	
			Cycles		3 rotations	
			Travel		3	
				2D/3D	3D	
		Permanent Offset				
	Target					
		Pinning				
			Pin Pressure		32%	32%
			Speed		19 mm per sec	19 mm per sec
			Backoff			
			Overshoot		2 mm	2 mm
			Repeat Pin		1 times	1 times
		Dry Mix				
			Clearance		0.5 mm	0.5 mm
			Diameter		1 mm	1 mm
			Cycles		1 rotations	1 rotations
		Wet Mix				
			Diameter			
			Speed			
			Cycles			
			Travel			
				2D/3D		
	Pads					
		Pressure				
		Eject Time				
	Selected Options					
		Recycle			Off	Off
		Revist			Off	Off
		Protect Source			Off	Off
		Offset				Auto
		Source Mix			On	On
		Target Mix			On	Off

126 **Table S2.** Mass spectrometry analysis confirms that the growth medium is not contaminated with
127 organosulfurs. ND= Not Detected. See **Materials and Methods**.
128

	Cysteine	Methionine	Homocysteine	SAM
Yeast Nitrogen Base	ND	ND	ND	ND
2% Glucose	ND	ND	ND	ND
Leucine	ND	ND	ND	ND
Histidine	ND	ND	ND	ND
Uracil	ND	ND	ND	ND
Lysine	ND	ND	ND	ND
Glutamic Acid	ND	ND	ND	ND
SD-Met	ND	ND	ND	ND
SD+Met	ND	7.15 mM	ND	ND
ddH_2O	ND	ND	ND	ND
Pure H_2O	ND	ND	ND	ND

129

Table S3. *YLL058W* and its orthologs are found in a cluster of genes near the telomere. *S. cerevisiae* gene names are used for all species shown. The ten nearest genes (5 upstream (5') genes, numbered -1 to -5, and 5 downstream (3') genes, numbered 1 to 5) to *YLL058W* orthologs are shown. Asterisks indicate a known role in sulfur metabolism.

		Position Relative to YLL058W										
		-5	-4	-3	-2	-1	*YLL058W*	1	2	3	4	5
Species	*Saccharomyces cerevisiae*	*PAU18*	*AYT1*	*MHT1**	*MMP1**	*GTT2**	*YLL058W**	*JLP1**	*YLL056C*	*YCT1**	*YLL054C*	*YLL053C*
	Zygosaccharomyces bisporus	*RRP42*	*TRM3*	*ATG20*	*YDL114W*	*ARG8*	*YLL058W**	*YLL058W**	*YCT1**	*AYR1*	*DAL5*	*PUT3*
	Torulaspora delbrueckii	*RPT6*	*ALG23*	*DSE4*	*MHT1**	*MMP1**	*YLL058W**	*YCT1**	*DLD2*	*GRX1**	*DIP5*	*YRF1-1*
	Torulaspora pretoriensis	*THI73*	*AMD2*	*SOA1**	*JLP1**	*PHO84*	*YLL058W**	*MMP1**	*MHT1**	*DSE4*	*ALG23*	*RPT6*
	Lachancea quebecensis	*YCT1**	*SOA1**	*ZRT1*	*PHO11*	*ZPS1*	*YLL058W**	*VEL1*	*FLO5*	*COS9*	*AIF1*	*YER152C*

136 **Table S4.** OD_{600} values at saturation (~51 hours) for cultures of the indicated strains grown in SD-
137 Met+Glu medium with or without the H_2S chelator Ferric(Fe)-EDTA (column 4), and OD_{600} values for the
138 same cultures diluted and repassaged in SD-Met-Glu medium lacking chelator (column 5). Each strain
139 has 3 replicates (1-3) from two independent experiments (A&B). Although FY4-*met15Δ* cultures generally
140 failed to show any substantial growth in liquid medium without an H_2S chelator present (**Figure 4B**), we
141 occasionally observed "escape" in four FY4-*met15Δ* cultures (indicated in green text) grown in SD-
142 Met+Glu without an H_2S chelator present, independent of whether the cells had previously been in the
143 presence of chelator.
144

Strain	Replicate	Initial Medium	OD600	OD600 (Repassage)
FY4	1A	SD-Met+Glu	4.98	6.13
FY4	1B	SD-Met+Glu	5.45	4.75
FY4	2A	SD-Met+Glu	4.9	5.88
FY4	2B	SD-Met+Glu	5.71	4.64
FY4	3A	SD-Met+Glu	5.13	6.45
FY4	3B	SD-Met+Glu	5.76	5.8
FY4	1A	SD-Met+Glu+Fe-EDTA	5.86	7.71
FY4	1B	SD-Met+Glu+Fe-EDTA	6.76	7.03
FY4	2A	SD-Met+Glu+Fe-EDTA	5.5	7.82
FY4	2B	SD-Met+Glu+Fe-EDTA	6.24	6.78
FY4	3A	SD-Met+Glu+Fe-EDTA	5.26	7.87
FY4	3B	SD-Met+Glu+Fe-EDTA	6.15	6.61
FY4-*met15Δ*	1A	SD-Met+Glu	1.39	0.48
FY4-*met15Δ*	1B	SD-Met+Glu	0.21	0.09
FY4-*met15Δ*	2A	SD-Met+Glu	0.29	5.93
FY4-*met15Δ*	2B	SD-Met+Glu	0.22	0.07
FY4-*met15Δ*	3A	SD-Met+Glu	0.34	0.14
FY4-*met15Δ*	3B	SD-Met+Glu	0.21	0.07
FY4-*met15Δ*	1A	SD-Met+Glu+Fe-EDTA	2.55	0.39
FY4-*met15Δ*	1B	SD-Met+Glu+Fe-EDTA	1.02	3.29
FY4-*met15Δ*	2A	SD-Met+Glu+Fe-EDTA	2.23	0.26
FY4-*met15Δ*	2B	SD-Met+Glu+Fe-EDTA	0.56	0.08
FY4-*met15Δ*	3A	SD-Met+Glu+Fe-EDTA	2.52	4.22
FY4-*met15Δ*	3B	SD-Met+Glu+Fe-EDTA	1.12	3.32

145

146 **Table S5.** Kruskal-Wallis Test results comparing the growth of a given strain in condition_1 (+Met) vs.
147 condition_2 (-Met), with EtOH or Glucose. The statistic and p-value columns are the Kruskal-Wallis test
148 statistic and p-value output, and the effect size column is the difference between the median fitness value
149 in media lacking methionine and that in media containing methionine divided by the median fitness value
150 in media containing methionine.
151

Strain	condition_1 (+Met)	condition_2 (-Met)	statistic	p-value	effect size
FY4	SD+Met+EtOH	SD-Met+EtOH	0.0300	0.8625	0.0000
FY4-*met15Δ*	SD+Met+EtOH	SD-Met+EtOH	17.2800	0.0000	-0.8926
FY4-*met15Δ* (ρ–)	SD+Met+EtOH	SD-Met+EtOH	12.5952	0.0004	-0.4500
FY4 (ρ–)	SD+Met+EtOH	SD-Met+EtOH	0.4821	0.4875	0.1471
FY4	SD+Met+Glu	SD-Met+Glu	0.3333	0.5637	0.0000
FY4-*met15Δ*	SD+Met+Glu	SD-Met+Glu	17.2800	0.0000	-0.6168
FY4-*met15Δ* (ρ–)	SD+Met+Glu	SD-Met+Glu	17.2800	0.0000	-0.4874
FY4 (ρ–)	SD+Met+Glu	SD-Met+Glu	3.8533	0.0496	-0.0683

152

153 **Table S6.** *Saccharomyces cerevisiae* strains used in this study (related to **Materials and Methods**).
154

Strain #	Strain name	Genotype	Used in Figure(s)	Source
yARC0052	BY4741	*MAT***a** *his3Δ1 leu2Δ0 met15Δ0 ura3Δ0*	1B, 1C, 1E, 1F, S2, S3A, S4A	Winzeler et al., 1999 (acquired from Horizon Discovery)
yARC0053	BY4742	*MAT α his3Δ1 leu2Δ0 lys2Δ0 ura3Δ0*	1B, 1C, 1E, 1F, S2, S3A, S4A	Winzeler et al., 1999 (acquired from Horizon Discovery)
yARC0055	BY4741 *HOΔ0 ::KanMX*	*MAT***a** *his3Δ1 leu2Δ0 met15Δ0 ura3Δ0 HOΔ0::KanMX*	S1	Giaever et al., 2002
yARC0056	BY4742 *HOΔ0 ::KanMX*	*MAT α his3Δ1 leu2Δ0 lys2Δ0 ura3Δ0 HO::KanMX*	S1	Giaever et al., 2002
yARC0083	FY4	*MAT***a**	1G, 2B, 2C, 2D, 2E, 4B, 4C, 4E, S2, S3A, S3B, S4, S5A, S5B, S8, S10	Winston et al., 1995
yARC0293	FY4-*cys4Δ0*	*MAT***a** *cys4Δ0*	2B, 2C, 2D, S5A	This Study
yARC0224	FY4-*met2Δ0*	*MAT***a** *met2Δ0*	2B, 2C, 2D, S5A, S5B	This Study
yARC0312	FY4-*met3Δ0*	*MAT***a** *met3Δ0*	2B, 2C, 2D, 2E, S4, S5A, S5B	This Study
yARC0458	FY4-*met5Δ0*	*MAT***a** *met5Δ0*	2B, 2C, 2D, S5A, S5B	This Study
yARC0300	FY4-*met6Δ0*	*MAT***a** *met6Δ0*	2B, 2C, 2D, S5A, S5B	This Study
yARC0459	FY4-*met10Δ0*	*MAT***a** *met10Δ0*	2B, 2C, 2D, S5A, S5B	This Study
yARC0222	FY4-*met12Δ0*	*MAT***a** *met12Δ0*	2B, 2C, 2D, S5A, S5B	This Study
yARC0310	FY4-*met13Δ0*	*MAT***a** *met13Δ0*	2B, 2C, 2D, S5A, S5B	This Study
yARC0178	FY4-*met15Δ0*	*MAT***a** *met15Δ0*	1G, 2B, 2C, 2D, 2E, 4B, 4C, 4E, S2, S3A, S3B, S5A, S5B, S10	This Study
yARC0295	FY4-*str3Δ0*	*MAT***a** *str3Δ0*	2B, 2C, 2D, S5A, S5B	This Study
yARC0220	FY4-*yll058wΔ0*	*MAT***a** *yll058wΔ*	S8	This Study
yARC0460	FY4	*MAT***a** *pGDP-ccdB::KanMx*	3D	This Study
yARC0461	FY4-*met15Δ0*	*MAT***a** *met15Δ0 pGDP-ccdB::KanMx*	3D	This Study
yARC0462	FY4-*yll058wΔ0*	*MAT***a** *yll058wΔ pGDP-ccdB::KanMx*	3D	This Study
yARC0463	FY4- *met15Δ0 yll058wΔ0*	*MAT***a** *met15Δ0 yll058wΔ pGDP-ccdB::KanMx*	3D	This Study
yARC0464	FY4-*met15Δ0*	*MAT***a** *met15Δ0 pGDP-yll058w::KanMx*	3D	This Study
yARC0465	FY4- *met15Δ0 yll058wΔ0*	*MAT***a** *met15Δ0 yll058wΔ pGDP-yll058w::KanMx*	3D	This Study
yARC0207	FY4 (ρ-)	*MAT***a** *(ρ-)*	4D, 4E	This Study
yARC0208	FY4-met15Δ (ρ-)	*MAT***a** *met15Δ0 (ρ-)*	4D, 4E	This Study

155
156

157 **Table S7.** Plasmids used in this study (related to **Materials and Methods**).
158

Plasmid #	Construction	Yeast Origin	Promoter	Gene Product(s)	Markers	Used in Figure(s)
pARC0028	See (Ryan et al., 2014)	2μ		Cas9+sgRNA	KanR	
pARC0112	LEU2 was replaced by *KanMX* on plasmid pAG425GPD-ccdB from Yeast Gateway Kit (Alberti et al., 2007)	2μ	GPD	ccdB (empty plasmid)	G418R (*KanMX*)	3D
pARC0172	Made by LR recombination between destination plasmid pARC0112 and entry clone containing the YII058w gene cds	2μ	GPD	YII058w	G418R (KanMX)	3D
pARC0190	The coding sequence for *MET15* was amplified from *S. cerevisiae* genomic DNA and cloned into a pET28a-derived vector expressing an N-terminal, cleavable 10XHis-Ruby (Kredel et al., 2009) tag.		T7	10XHis-Ruby-TEV-Met15	KanR	S11
pARC0191	The coding sequence for YLL058W was amplified from *S. cerevisiae* genomic DNA and cloned into a pET28a-derived vector expressing an N-terminal, cleavable 10XHis-Ruby (Kredel et al., 2009) tag.		T7	10XHis-Ruby-TEV-YII058w	KanR	S11

159

160 **Table S8.** sgRNA, repair fragment template (HR_template) and amplification primer (HR_Fw and HR_rv)
161 sequences used for CRISPR/Cas9-mediated ORF deletions (related to **Materials and Methods**).
162

ORF name	Primers	Sequence	Used to construct strain #
CYS4	sgRNA	GTTGTAGGCCACTTGCTCAA	yARC0293
	HR_template	CATCTAGATAAATACGACGTAAGAATAAAAATAAGAACCCACGCTTCAAATAAAAGCAAA	
	HR_Fw	AGTAAAAGGCAACACTTGAAGATTTCGTTGTAGGCCACTTGCTCAAACGACATCTAGATA	
	HR_Rv	AGAGAACGGTGCAATTGAATAGGAAAGGAATGACGGATTTTGCTTCTATGTTTGCTTTTA	
MET2	sgRNA	ATCGAAAACGCTCCAAGAGC	yARC0224
	HR_template	AAAGAAAGAAAAAAACGTAGTATAAAAGGAGGATAGATACCACACATACCTCAGGCATAA	
	HR_Fw	TTTTTAGTCACAGGGTCCGTCTAAAGTTTCTCTTTATTTGGAATAATAGAAAAGAAAGAA	
	HR_Rv	GAAAGGACCTCAGTGATGTCATCTACTCTGTCTCTTGCCAAATCGTGCGTATCCAGTTTA	
MET3	sgRNA	AACATGCCTGCTCCTCACGG	yARC0312
	HR_template	TAATAATAACAAGAATAAAGTATAATTAACTCGTCATAAAATGCTCCCATCTCAAAAGTA	
	HR_Fw	ACTTATTTGCAAATCTATTTATTTTGCGCGGTCGATCATGAATTTTGCCCTACTTTTGAG	
	HR_Rv	ACTTATTTGCAAATCTATTTATTTTGCGCGGTCGATCATGAATTTTGCCCTACTTTTGAG	
MET5	sgRNA	ACAATTGTGGGAGCGTCAAG	yARC0458
	HR_template	TAGTATGTCCTACTATGTCATATGCTATCATCGCCAATCTTTTGTTTTTCTCTGGTTCCC	
	HR_Fw	AGTTATATTCAATTGCGAAAAAAATAAATAAATGTGGGAAGAAAACCCAATAGTATGTCC	
	HR_Rv	TTGATATTTATTCAGATCCCTTATATACTAATAAAGTAACAGTAGGGAACGGGAACCAGA	
MET6	sgRNA	TTCAAAGTACATATCAAAAA	yARC0300
	HR_template	ACCAATATAATTTCAAAGTACATATCAAAAGGTTTTAAAAAGGAAGCAAAGTAATGATAT	
	HR_Fw	ATAAAAAAGCAAGCATCTAAGAGCATTGACAACACTCTAAGAAACAAAATACCAATATAA	
	HR_Rv	ATTAAATCACCGATGTTGAATCCCAGAATAAAAAACAAAAAGTTCAGAAAATATCATTAC	
MET10	sgRNA	GGATTGGTAGCAAACTCAAC	yARC0459
	HR_template	TAGATATTTAGTTTTTATTACTATATTAATCTCGTTGTATATTTGGGTGACCTCGAGGAA	
	HR_Fw	AAAACTAAAAGTAAAAAAAAAATAGAAATGTTCAAGACAGGTTCAATAAATAGATATTTA	
	HR_Rv	TGGAAATAGTTTCGTTTAGATGGGGTGCACATAGTTTTTTTCAACTGCTTTTCCTCGAGG	
MET12	sgRNA	TCAGAGATTTATATCATGCG	yARC0222
	HR_template	GACGGGACAGGTTGATTACATTTTTTAAACTATTTCACTGAATATAAATACAAAAATGCG	
	HR_Fw	CTCACATCATCTATTTTGTTTCAAGTTCGTACATTTTTTGAAGCGTGTTGGACGGGACAG	
	HR_Rv	TTAGAAGGGCGTTCTGCCCGTTATGTATACGTTAAATATTACATTATTTTCGCATTTTTG	
MET13	sgRNA	GAGCAACATAGACAGACCTC	yARC0310
	HR_template	CCACAGTTACTACTACAACCACATCGCAATTAACACAGACAACGATAACAGTTCTTTAAC	
	HR_Fw	CCTTGATTGAAATAGTCTCCCTAAACTAAAGTTATCAGCAAACAGAACCACCACAGTTAC	
	HR_Rv	AATGCAATGTAATGTTGAATGTAATGCAAAGAGGGGGGGTTGACAATTCTGTTAAAGAAC	
MET15	sgRNA	GATACTGTTCAACTACACGC	yARC0178
	HR_template	AGATACAATTCTATTACCCCCATCCATACAGTGTGCGTAATGAGTTGTAAAATTATGTAT	
	HR_Fw	GTCTTTTCATCTACTATTTCCTTCGTGTAATACAGGGTCGTCAGATACATAGATACAATT	
	HR_Rv	AATAAAGTTCGTTTTATAAAAGTATAGTACTTGTGAGAGAAAGTAGGTTTATACATAATT	
STR3	sgRNA	CAAGAGATTAGATACAGTTG	yARC0295
	HR_template	agcaaacaacaaaagcatagaagcaaaaagGGGAAAATATGCATGTACCtttttttttt	
	HR_Fw	ACATCCCATAGCTCTGTGTGCTTACAGTTCATTaaaaacaaaaaatatcaagcaaacaac	
	HR_Rv	TATACTTGACTATTTAAAGTTACTATCTTTGGATTTGAACCTTATaaaaaaaaaaaaaaa	
YLL0558W	sgRNA	TGAACAACTATTAATCATCG	yARC0220
	HR_template	GAACAACTATTAATCATCGTGGAAATTATTAGCAGATCATGAGTAGAATATCAAAAATCA	
	HR_Fw	TCTCTGGTGCGGTAAAACATAAATTTTAAATCTAGTACTCAACCACCACTGAACAACTAT	
	HR_Rv	TGGAAAAAAACTTTTATAAACAATATTCTATAAAGATTATAAAGAATTCTTGATTTTTGA	

163

164 **Table S9.** Yeast growth conditions in this study (related to **Materials and Methods**). When required, the
165 analogous liquid medium was made with the same composition, excluding the 2% agar.
166

Growth Conditions	Composition	Used in Figure(s)
BiGGY	10.0 g/L glucose	2C, 2D, 4C, S8B, S8C
	10.0 g/L glycine	
	1.0 g/L yeast extract	
	3.0 g/L Na2SO4	
	2.5 g/L bismuth ammonium citrate	
	2 % Agar	
Homemade YNB – Inorganic Sulfates (SD-Met+Glu)	200 ul/L of Vitamin Stock (5000x)	2E
	200 ul/L of Trace Elements Stock (10 000x)	
	10 ml/L of Salt Stock (100x)	
	2.0 g/L '-met-cys+ura' drop-out (+histidine, +leucine, +lysine, +uracil)	
	1 g/L L-glutamic acid	
	2 % Glucose/Galactose	
	2 % agar	
Homemade YNB + Inorganic Sulfates (SD-Met+Glu)	200 ul/L of Vitamin Stock (5000x)	2E
	200 ul/L of Trace Elements Stock (10 000x)	
	10 ml/L of Salt Stock (100x)	
	2.0 g/L '-met-cys+ura' drop-out (+histidine, +leucine, +lysine, +uracil)	
	1 g/L L-glutamic acid	
	2 % Glucose/Galactose	
	2 % agar	
SC-Leu+Glu	1.7 g/L Yeast Nitrogen Base without amino acids and ammonium sulfate	S2
	2.0 g/L SC drop-out (-leucine)	
	1 g/L L-glutamic acid	
	2 % Galactose	
	2 % Agar	
SC-Met-Cys+Glu	1.7 g/L Yeast Nitrogen Base without amino acids and ammonium sulfate	4C, S2
	2.0 g/L SC drop-out (-methionine, -cysteine)	
	1 g/L L-glutamic acid	
	2 % Glucose	
	2 % Agar	
SC-Met-Cys+Gal	1.7 g/L Yeast Nitrogen Base without amino acids and ammonium sulfate	S2
	2.0 g/L SC drop-out (-methionine, -cysteine)	
	1 g/L L-glutamic acid	
	2 % Galactose	
	2 % Agar	
SD-Met+EtOH	1.7 g/L Yeast Nitrogen Base without amino acids and ammonium sulfate	1C, 4E, S3B, S4
	2.0 g/L '-met-cys' drop-out (+histidine, +leucine, +lysine, +uracil)	
	1 g/L L-glutamic acid	
	3 % Ethanol	
	2 % Agar	
SD-Met+Gal	1.7 g/L Yeast Nitrogen Base without amino acids and ammonium sulfate	1C, 3D, S3B, S4
	2.0 g/L '-met-cys' drop-out (+histidine, +leucine, +lysine, +uracil)	
	1 g/L L-glutamic acid	
	2 % Galactose	
	2 % Agar	
SD-Met+Glu	1.7 g/L Yeast Nitrogen Base without amino acids and ammonium sulfate	1B, 1C, 1E, 1F, 1G, 2B, 4B, 4C, 4D, 4E, S1, S3A, S3B, S4, S8A
	2.0 g/L '-met-cys' drop-out (+histidine, +leucine, +lysine, +uracil)	
	1 g/L L-glutamic acid	
	2 % Glucose	
	2 % Agar	
SD-Ura+EtOH	1.7 g/L Yeast Nitrogen Base without amino acids and ammonium sulfate	1C, S3B, S4
	2.0 g/L '+met-cys-ura' drop-out (+histidine, +leucine, +lysine, +methionine)	
	1 g/L L-glutamic acid	
	3 % Ethanol	
	2 % Agar	
SD-Ura+Gal	1.7 g/L Yeast Nitrogen Base without amino acids and ammonium sulfate	1C, S3B, S4
	2.0 g/L '+met-cys-ura' drop-out (+histidine, +leucine, +lysine, +methionine)	
	1 g/L L-glutamic acid	
	2 % Galactose	
	2 % Agar	

167

SD-Ura+Glu	1.7 g/L Yeast Nitrogen Base without amino acids and ammonium sulfate	1C, S3B, S4
	2.0 g/L '+met-cys-ura' drop-out (+histidine, +leucine, +lysine, +methionine)	
	1 g/L L-glutamic acid	
	2 % Glucose	
	2 % Agar	
SD-Leu+Glu	1.7 g/L Yeast Nitrogen Base without amino acids and ammonium sulfate	1C, S3B
	2.0 g/L '+met-cys-leu' drop-out (+histidine, +uracil, +lysine, +methionine)	
	1 g/L L-glutamic acid	
	2 % Glucose	
	2 % Agar	
SD+Met+EtOH	1.7 g/L Yeast Nitrogen Base without amino acids and ammonium sulfate	4E
	2.0 g/L '+met-cys' drop-out (+histidine, +leucine, +lysine, +methionine)	
	1 g/L L-glutamic acid	
	2 % Glucose	
	2 % Agar	
	2 % Agar	
SD+Met+Glu	1.7 g/L Yeast Nitrogen Base without amino acids and ammonium sulfate	1C, 2E, 4D
	2.0 g/L '+met-cys' drop-out (+histidine, +leucine, +lysine, +uracil, +methionine)	
	1 g/L L-glutamic acid	
	2 % Glucose	
	2 % Agar	
SD-Met+Bi+Glu	1.7 g/L Yeast Nitrogen Base without amino acids and ammonium sulfate	S5A, S5B, S8B, S8C
	2.0 g/L '-met-cys' drop-out (+histidine, +leucine, +lysine, +uracil)	
	1 g/L L-glutamic acid	
	2 % Glucose	
	2 % Agar	
	2.5 g/L bismuth ammonium citrate	
YPDA	20 g/L Peptone	2B, 4C, S8A
	10 g/L Yeast Extract	
	2 % Galactose	
	120 mg/L Adenine	
	2 % Agar	
SC-Met-Cys+(Fe)EDTA+Glu	1.7 g/L Yeast Nitrogen Base without amino acids and ammonium sulfate	4C
	2.0 g/L SC drop-out (-methionine, -cysteine)	
	1 g/L L-glutamic acid	
	2 % Glucose	
	2 % Agar	
	0.048M Fe-EDTA	
SD-Met+(Fe)EDTA+Glu	1.7 g/L Yeast Nitrogen Base without amino acids and ammonium sulfate	4B, S10
	2.0 g/L '-met-cys' drop-out (+histidine, +leucine, +lysine, +uracil)	
	1 g/L L-glutamic acid	
	2 % Glucose	
	2 % Agar	
	0 - 0.136M Fe-EDTA	
SD+His+Leu+Ura+Glu	1.7 g/L Yeast Nitrogen Base without amino acids and ammonium sulfate	S1
	2.0 g/L drop-out (+histidine, +leucine, +uracil)	
	1 g/L L-glutamic acid	
	2 % Glucose	
	2 % Agar	
GNA	50 g/L Glucose	S1
	30 g/L Difco Nutrient Broth	
	10 g/L Yeast Extract	
	2 % agar	
SPO	10 g/L Glucose	S1
	1.25 g/L Yeast Extract	
	10 g/L Potassium Acetate	
	10 ml/L (100mM lysine)	
	3 mL/L (100mM histidine)	
	2 % agar	

168

Homemade Yeast Nitrogen Base without Inorganic Sulfate	
Component	**Concentration**
	Vitamins
Biotin	2µg/L
Calcium Pantothenate	400µg/L
Folic Acid	2µg/L
Inositol	2,000µg/L
Niacin	400µg/L
p-Aminobenzoic Acid	200µg/L
Pyridoxine Hydrochloride	400µg/L
Riboflavin	200µg/L
Thiamine Hydrochloride	400µg/L
	Trace Elements
Boric Acid	500µg/L
Cupric chloride	37.74µg/L
Potassium Iodide	100µg/L
Ferric Chloride	200µg/L
Manganese Chloride	333.34µg/L
Sodium Molybdate	200µg/L
Zinc Sulfate	400µg/L
	Salts
Monopotassium Phosphate	1.0g/L
Magnesium Chloride	0.395g/L
Sodium Chloride	0.1g/L
Calcium Chloride	0.1g/L

Homemade Yeast Nitrogen Base with Inorganic Sulfate	
Component	**Concentration**
	Vitamins
Biotin	2µg/L
Calcium Pantothenate	400µg/L
Folic Acid	2µg/L
Inositol	2,000µg/L
Niacin	400µg/L
p-Aminobenzoic Acid	200µg/L
Pyridoxine Hydrochloride	400µg/L
Riboflavin	200µg/L
Thiamine Hydrochloride	400µg/L
	Trace Elements
Boric Acid	500µg/L
Copper Sulfate	40µg/L
Potassium Iodide	100µg/L
Ferric Chloride	200µg/L
Manganese Sulfate	400µg/L
Sodium Molybdate	200µg/L
Zinc Sulfate	400µg/L
	Salts
Monopotassium Phosphate	1.0g/L
Magnesium Sulfate	0.5g/L
Sodium Chloride	0.1g/L
Calcium Chloride	0.1g/L

172 **SUPPLEMENTARY REFERENCES**
173
174 Alberti, S., Gitler, A.D., and Lindquist, S. (2007). A suite of Gateway cloning vectors for
175 high-throughput genetic analysis in Saccharomyces cerevisiae. Yeast *24*, 913-919.
176 10.1002/yea.1502.
177 Brewster, J.L., Pachl, P., McKellar, J.L.O., Selmer, M., Squire, C.J., and Patrick, W.M.
178 (2021). Structures and kinetics of Thermotoga maritima MetY reveal new insights into
179 the predominant sulfurylation enzyme of bacterial methionine biosynthesis. J Biol Chem
180 *296*, 100797. 10.1016/j.jbc.2021.100797.
181 Butcher, R.A., Bhullar, B.S., Perlstein, E.O., Marsischky, G., LaBaer, J., and Schreiber,
182 S.L. (2006). Microarray-based method for monitoring yeast overexpression strains
183 reveals small-molecule targets in TOR pathway. Nat Chem Biol *2*, 103-109.
184 10.1038/nchembio762.
185 Douglas, A.C., Smith, A.M., Sharifpoor, S., Yan, Z., Durbic, T., Heisler, L.E., Lee, A.Y.,
186 Ryan, O., Gottert, H., Surendra, A., et al. (2012). Functional analysis with a barcoder
187 yeast gene overexpression system. G3 (Bethesda) *2*, 1279-1289.
188 10.1534/g3.112.003400.
189 Giaever, G., Chu, A.M., Ni, L., Connelly, C., Riles, L., Veronneau, S., Dow, S., Lucau-
190 Danila, A., Anderson, K., Andre, B., et al. (2002). Functional profiling of the
191 Saccharomyces cerevisiae genome. Nature *418*, 387-391. 10.1038/nature00935.
192 Kredel, S., Oswald, F., Nienhaus, K., Deuschle, K., Rocker, C., Wolff, M., Heilker, R.,
193 Nienhaus, G.U., and Wiedenmann, J. (2009). mRuby, a bright monomeric red
194 fluorescent protein for labeling of subcellular structures. PLoS One *4*, e4391.
195 10.1371/journal.pone.0004391.

196 Lu, H., Li, F., Sanchez, B.J., Zhu, Z., Li, G., Domenzain, I., Marcisauskas, S., Anton,
197 P.M., Lappa, D., Lieven, C., et al. (2019). A consensus S. cerevisiae metabolic model
198 Yeast8 and its ecosystem for comprehensively probing cellular metabolism. Nat
199 Commun *10*, 3586. 10.1038/s41467-019-11581-3.
200 Winston, F., Dollard, C., and Ricupero-Hovasse, S.L. (1995). Construction of a set of
201 convenient Saccharomyces cerevisiae strains that are isogenic to S288C. Yeast *11*, 53-
202 55. 10.1002/yea.320110107.
203 Winzeler, E.A., Shoemaker, D.D., Astromoff, A., Liang, H., Anderson, K., Andre, B.,
204 Bangham, R., Benito, R., Boeke, J.D., Bussey, H., et al. (1999). Functional
205 characterization of the S. cerevisiae genome by gene deletion and parallel analysis.
206 Science *285*, 901-906. 10.1126/science.285.5429.901.
207
208